Published in final edited form as:

Nature. 2024 November ; 635(8040): 935–942. doi:10.1038/s41586-024-08075-8.

Neuronal Sequences in Population Bursts Encode Information in Human Cortex

Weizhen Xie[1,2,*,†], **John H. Wittig Jr**[1,*], **Julio I. Chapeton**[1], **Mostafa El-Kalliny**[1], **Samantha N. Jackson**[1], **Sara K. Inati**[1], **Kareem A. Zaghloul**[1,†]

[1]Surgical Neurology Branch, NINDS, National Institutes of Health, Bethesda, MD 20892, USA

[2]Department of Psychology, University of Maryland, College Park, MD 20742, USA

Summary

Neural coding has traditionally been examined through changes in firing rates and latencies in response to different stimuli[1-5]. However, populations of neurons can also exhibit transient bursts of spiking activity, wherein neurons fire in a specific temporal order or sequence[6-8]. The human brain may utilize these neuronal sequences within population bursts to efficiently represent information[9-12], thereby complementing the well-known neural code based on spike rate or latency. Here, we examine this possibility by recording the spiking activity of populations of single units in the human anterior temporal lobe (ATL) as eight participants perform a visual categorization task. We find that population spiking activity organizes into bursts during the task. The temporal order of spiking across the activated units within each burst varies across stimulus categories, creating unique stereotypical sequences for individual categories as well as for individual exemplars within a category. The information conveyed by the temporal order of spiking activity is separable from and complements the information conveyed by the units' spike rates or latencies following stimulus onset. Collectively, our data provide evidence that the human brain contains a complementary code based on the neuronal sequence within bursts of population spiking to represent information.

Introduction

Changes in firing rate and the spike latency following stimulus onset have traditionally been regarded as prominent and correlated neural coding schemes that support diverse behavioral and cognitive phenomena[1-5]. Previous studies have also suggested that stimuli can evoke a transient and coordinated burst of spiking among an assembly of neurons[6,7]. These bursts may reflect discrete packets of information[6], serving as transient pulses to facilitate information transmission across neocortical networks[13,14]. While it is unclear how

†Corresponding authors Kareem A. Zaghloul; kareem.zaghloul@nih.gov; Weizhen Xie; zanexie@umd.edu.
*Denotes equal contribution

Author contributions

Conceptualization: KAZ, WX, JHW; Methodology: JHW, WX, ME, SNJ, KAZ; Software: JWH, WX; Validation: WX; Formal Analysis: JHW, WX, JIC; Investigation: JHW, WX, JIC, SKI, KAZ; Resources: KAZ; Data Curation: JHW, WX, SJ; Writing-Original Draft: WX; Writing-Review and Editing: KAZ, WX, JHW, JIC; Visualization: WX, JHW, JIC; Supervision: KAZ.

Conflict of interest

The authors declare no competing financial interests.

the brain might use these bursts to convey information[13,15], the temporal order of spiking activity within these bursts, or the neuronal sequence, could provide a complementary neural code. By leveraging the combinatorial power of relative spike timing to encode complex information using only sparse spiking activity, information coding based on neuronal sequences may improve the brain's computational efficiency[9-12]. Despite this possibility, however, relatively little is known about how neuronal sequences within bursts of spiking contribute to human cognition.

Neuronal sequences within bursts of spiking across a population of neuronal units have long been observed in awake and behaving animals[6,16,17]. Because these bursts have a short temporal duration (e.g., 50-150ms), the sequences nested within them differ from the sequential neural activity evoked by time-evolving experiences, such as when an animal traverses different paths in an environment[18], sniffs air with different odors[19], coordinates different motor actions[20], or views dynamically changing visual stimuli[21]. Prior research linking these neuronal sequences within population bursts to information coding has primarily relied on recordings from animal primary sensory cortices using basic stimulus features such as gratings with different orientations[17] or tones with different frequencies[6]. It remains unclear how neuronal sequences within population bursts in association regions of the neocortex, particularly in the human brain, may contribute to the encoding of information across different levels of a representational hierarchy, a hallmark of higher-order cognition[22].

Here, we examine sequences of neuronal firing within discrete spiking bursts across a population of neuronal units recorded from the human ATL as participants perform a visual categorization task. Based on the hypothesized role of neuronal sequences in coding information[11], we predicted that the order of spikes from recorded neuronal units within population bursts should be sufficient for representing information across different visual categories and among exemplars within a chosen category. Moreover, if these neuronal sequences complement other neural codes, the information encoded by neuronal sequences to support visual categorization should be distinct from that encoded by spike rate or its correlated measures such as spike latency from stimulus onset[1-5]. Our data support this hypothesis, demonstrating that neuronal sequences within population bursts in the human ATL carry non-redundant information regarding the taxonomic categories as well as individual exemplars of visually presented images. These findings therefore suggest that neuronal sequences within bursts of population spiking may serve as a complementary neural code for representing information in the human brain.

Results

We recorded activity of populations of ATL neurons in 8 participants (36.25 ± 3.38 years old, 3 females, IQ: 86.50 ± 5.35; see Supplementary Table S1) as they performed a visual categorization task (Fig. 1a). In this task, participants view an image presented on the screen for 500 ms and provide a categorical judgment of the image from one of the four taxonomic categories (ANIMAL, OBJECT, PERSON, and PLACE; 951 ± 121 trials; Extended Data Fig. 1a) or from one of the four exemplars of a predefined category (i.e., four different US presidents within the PERSON category; 245 ± 29 of trials; Extended Data Fig. 1b). The

inclusion of both taxonomic and exemplar categorization allows us to determine whether neuronal sequences within bursts of spiking encode information across different levels of a representation hierarchy. To rule out the possibility that the recorded units only encode motor responses instead of the information content associated with the stimuli, a subset of participants also completed a set of control trials (66 ± 6 trials; Extended Data Fig. 1c). During these control trials, participants indicate the direction of a low-contrast arrow presented on the screen from one of the four possible directions (UP, DOWN, LEFT, RIGHT). Participants performed these different types of trials in sequential blocks (arrows, taxonomic, and then president trials) while other experimental factors such as image order and stimulus categories were randomly intermixed within each block. As accuracy is emphasized over speed, participants' performance is high with an average accuracy of 95.9% ± 1.0% for taxonomic categorization (correct response time, RT = 1039 ms ± 70 ms), 95.0% ± 1.7% for president/exemplar categorization (RT = 1100 ms ± 56 ms), and 91.7% ± 3.0% for arrow direction categorization (RT = 1051 ms ± 70 ms; see Extended Data Fig. 1d).

We isolated a total of 2110 putative single units from 12 micro-electrode arrays[23,24] (MEAs; Fig. 1b) across 18 recordings (117 ± 13 units per recording; see Extended Data Fig. 1e). In an example array, a population spike raster demonstrates bursts of coordinated spiking across many units in almost every trial (Fig. 1c). These bursts tend to last a brief duration of 50-150 ms and exhibit no discernible relation with stimulus onset or response time. Moreover, these bursts exhibit variability in the number of spiking units across categories and varying spike counts from each unit within a burst. For instance, when an OBJECT image is presented in the current example, more units are activated during a burst and more spikes are produced overall as compared with those elicited by other categories.

Closer inspection of these bursts of spiking, however, reveals that spiking across the individual units is not perfectly synchronized. Spiking across the population of units within each category instead arises in a stereotypical temporal order or sequence. To illustrate this, we sort the units participating in a burst by their temporal order averaged across two example bursts elicited by different images from the same category. We find that during the presentation of images from the same category, the order of spiking activity across the population of participating units appears mostly retained (*upper* panel, Fig. 1d). This within-category sequence consistency is in contrast with the inconsistency in sequence order across categories. For example, when we resort all the example bursts based on the average order of the example bursts associated with OBJECT images, the sequential spiking patterns for bursts associated with ANIMAL, PERSON, and PLACE images are no longer retained (*lower* panel, Fig. 1d), suggesting some category specificity in units' spiking order. Combined, these observations suggest that bursts of population spiking activity may contain information about a visual image in various forms, for example, the number of spikes emitted by the set of units involved as well as the temporal order of spiking timing, or sequence[9,10], of these activated units within a burst.

Decoding based on Neuronal Sequences

Based on these observations and the previous evidence that groups of neurons activated during bursts of spiking tend to fire in a temporal order[6,25], we directly examined whether

the sequence of neuronal spiking within each burst could be used to decode information about the presented visual images. In each recording, we identified bursts of population spiking based on transient increases in the number of activated units. We compared these identified bursts in each individual recording with surrogate data generated from a random Poisson process to control for the false positive rate in burst detection (Extended Data Fig. 2a-b). All 18 recordings that we retained for our analyses demonstrate at least 100 bursts throughout the experiment (2504 ± 590 bursts per recording; 0.99 ± 0.19 bursts/second). These bursts appear to coincide with high-frequency (80-120 Hz) oscillatory events known as ripples recorded through the same cortical micro-electrodes (Extended Data Fig. 2e)[26].

To examine the order of neuronal sequences within these bursts, we assigned a rank to each unit based on the average spike time of each firing unit in that burst (Fig. 2a). Across units and bursts, the assigned rank for each unit is highly correlated with the spike latency from burst onset (τ_b, mean Spearman $\rho = 0.76$, range: 0.60 to 0.87), consistent with previous research that a unit's mean or peak spiking time can serve as a proxy for the temporal order of unit activity within a sequence[27,28]. We therefore used the rank for each unit to determine whether the order of neuronal spiking within bursts can be used to decode stimulus information. Because the timing of a unit's response may not always be relevant for information coding[2,3], we restricted our analyses to only those units that spike with a reliable normalized rank within bursts in response to at least one image category. We refer to these as sequence-related units (52.6% ± 4.8% of the recorded units per recording; Extended Data Fig. 3a-b). Note that this unit selection step is omnibus, imposing minimal assumptions for the specific relation between a unit's rank and the stimulus category. We then verified that neuronal sequences within a stimulus category are more similar than those across categories[29] (Fig. 2b). We created independent template neuronal sequences for each category by randomly selecting 20% of the bursts that occurred during each stimulus category for each fold of the data and averaging the normalized ranks of the sequence-related units within those bursts. Template sequences extracted separately for each taxonomic category are more similar to each other within the same category as compared those across different categories (Fisher's transformed Kendall's τ for within- and across-category similarity in mixed-effect modeling: 0.22 ± 0.02 vs. 0.17 ± 0.03, $t(34) = 7.07$, $p = 3.65e^{-08}$, $r_{equivalent} = 0.77$; Extended Data Fig. 3c).

To assess whether neuronal sequences within bursts can be used to decode information about the presented image, we used a template-matching approach[30]. Using a training set consisting of data from all but one burst, we constructed category-specific template sequences and predicted the category of the held-out test burst based on the template with the highest similarity between the training and test data (Fig. 2c). Accuracy of this leave-one-out classification for taxonomic categories at the burst level is significantly greater than chance across recordings (true vs. shuffled in mixed-effect modeling: 29.1% ± 0.70% vs. 25.0% ± 0.04%, $t(34) = 6.09$, $p = 6.64e^{-07}$, $r_{equivalent} = 0.72$, Fig. 2d). Decoding accuracy based on sequence order depends on the selection of units. Including units with less reliable ranks decreases classification accuracy (Extended Data Fig. 3d). Decoding of arrow trials based on spiking order is at chance level across 12 available recordings, confirming that neuronal sequences are not simply encoding motor mapping of different directions (true

vs. shuffled in mixed-effect modeling: 24.0% ± 2.8% vs. 25.0% ± 0.9%: $t(22) = -0.40$, $p = 0.69$, $r_{equivalent} = -0.09$; Extended Data Fig. 3e). Classification accuracy when decoding individual exemplars within the PERSON category is also significantly greater than chance despite reduced trial counts (true vs. shuffled in mixed-effect modeling: 29.0% ± 1.5% vs 24.7% ± 0.2%; $t(34) = 3.03$, $p = 0.0046$, $r_{equivalent} = 0.46$; Fig. 2d). Successful decoding of both taxonomic categories and the exemplars demonstrates that sequence coding within these spiking bursts occurs at multiple levels in the information representation hierarchy.

Consistent with prior research[31], we find that cortical units also show reliable increases or decreases in spike rate for images of a given stimulus category (Fig. 3a-b). As such, high-level visual information can be decoded from the patterns of population spike rates using a linear classifier (Extended Data Fig. 4). The overall classification accuracy based on spike rates during task period (100-1400 ms following stimulus onset) is significantly greater than the chance level for both taxonomic categories (true vs. shuffled in mixed-effect modeling: 38.8% ± 3.3% vs. 26.3% ± 0.4%, $t(34) = 4.45$, $p = 8.88e^{-05}$, $r_{equivalent} = 0.61$) and for exemplars within the PERSON category (33.1% ± 2.7% vs. 25.1% ± 0.3%, $t(34) = 3.56$, $p = 0.0011$, $r_{equivalent} = 0.52$; Fig. 3c), but not for the arrow trials (21.4% ± 1.6% vs. 24.4% ± 0.7%: $t(22) = -1.81$, $p = 0.083$, $r_{equivalent} = -0.36$; Extended Data Fig. 3e). These results, therefore, confirm that information about the presented images can also be encoded by spike rates in the human ATL.

Spiking Order is Separable from Rate

Our data demonstrate that spiking neurons in the human ATL can represent information to support visual categorization using both the sequential order of a bursting population of neuronal units and the pattern of population spike rates. Previous research has demonstrated that units that respond with higher spike rates are also more likely to fire with a shorter spike latency following stimulus onset[4,32]. Thus, one possibility is that the observed neuronal sequences within spiking bursts may be simply attributed to the strength of spiking responses.

To examine this possibility, it is important to first clarify the distinction between different measures of spike timing, one related to the onset of the stimulus and the other related to the onset of the population burst. To clarify this distinction, we visualized separately the raster plot of individual units across all trials and the response of all units on individual trials in an example recording (Fig. 4a). In this example, while individual units may not display a clear spiking response time-locked to stimulus onset, the population of units can exhibit highly coordinated spiking activity, manifesting as spiking bursts. We therefore explicitly examined the latency of a unit's first spike from stimulus onset, τ_o, and the latency of the first spike within a given burst, τ_b (Fig. 4b). Across all recorded units, the rank of each unit within a given spiking burst reflects the latency within the burst, τ_b (mean Spearman ρ = 0.76, range: 0.60 to 0.87), rather than the latency from stimulus onset, τ_o (mean Spearman $\rho = 0.06$, range: 0.02 to 0.11; Extended Data Fig. 5a). Moreover, overall spike rate during both task and baseline periods are robustly anticorrelated with the latency from stimulus onset, τ_o (e.g., mean Spearman ρ between task period spike rate and τ_o = -0.43, range: −0.51 to −0.33), consistent with previous findings[4,5]. However, this relation is markedly reduced

when examining the relation between spike rate and the units' relative rank within a burst sequence (mean Spearman ρ between task period spike rate and unit rank = −0.09, range: −0.16 to −0.02; Extended Data Fig. 5b). We also investigated the changes in spike rate and spike latency following stimulus onset to more directly examine whether the neuronal sequences during population bursts are related to the known relation between the strength of spiking response and spike latency from stimulus onset[4,32] (Extended Data Fig. 5c). We find that changes in spike rate are significantly correlated with latency from stimulus onset, τ_o, but not with the unit's rank within population bursts (Extended Data Fig. 5d). These differences in the correlations suggest that a neuronal unit's rank within population bursts is largely independent of its change in firing rate and spike latency from stimulus onset.

Closer examination of the known relation between spike rate and latency reveals that spike latency from stimulus onset, τ_o, in fact exhibits a systematic mean shift between different visual categories[32,33] (Fig. 4c). However, the relative order of τ_o across units is preserved across categories. Across recordings, the population mean of τ_o across sequence-related units in each trial can therefore be used to decode visual information more so than the rank order of τ_o using a similar template-based classification approach (trial-level decoding accuracy using mean vs. order of τ_o across units in mixed-effect modeling: 29.0% ± 0.7% vs. 26.8% ± 0.8%: $t(34) = 2.85$, $p = 0.0074$, $r_{equivalent} = 0.44$; Fig. 4d). In contrast, the ranks of these units within spiking bursts in the same trials capture stimulus category information through their relative order of spiking more so than the information captured through any shift of average rank within spiking bursts (trial-level decoding accuracy using mean vs. order of units' ranks: 24.8% ± 0.7% vs. 29.7% ± 0.8%: $t(34) = 5.64$, $p = 2.46e^{-6}$, $r_{equivalent} = 0.70$; also Extended Data Fig. 5e-f for using τ_b in replacement of spike rank). Comparing these two features of spike timing across units – the mean versus the relative order – we find a significant interaction effect on classification accuracy when we decode stimulus category using latency from stimulus onset (τ_o) versus the rank within spiking bursts in a mixed-effect model ($t(68) = 5.50$, $p = 6.28e^{-7}$, $r_{equivalent} = 0.55$). This suggests a dissociation between these two aspects of spike timing – mean population latency shifts versus rank order of the constituent units – and how they may differentially contribute to information coding.

Although the relative rank of neuronal firing within spiking bursts appears separable from spike latency from stimulus onset, it remains possible that the overall burst timing itself is sufficient to distinguish different visual categories. We thus also examined the time to burst onset within a trial, τ_{burst}. Across categories and recordings, τ_{burst} exhibits a relatively uniform distribution through the trial (Fig. 4e). The timing of the first bursts following stimulus onset per trial therefore does not significantly distinguish between taxonomic categories (true vs. shuffled in mixed-effect modeling: 25.9% ± 0.6% vs 24.9% ± 0.2%, $t(34) = 1.70$, $p = 0.10$, $r_{equivalent} = 0.28$). Moreover, decoding accuracy based on the neuronal sequences is unaffected by the timing of the held-out test burst during the trial (early, middle, and late spiking bursts relative to the trial RT: $F(2, 34) = 0.068$, $p = 0.93$) or whether bursts occurred during image presentation or not (image on vs. off: $t(34) = 1.25$, $p = 0.22$, $r_{equivalent} = 0.21$; Extended Data Fig. 3f). Thus, the stimulus information conveyed by units' spiking order within population bursts cannot be simply accounted for by burst timing[13,15].

Sequence and Rate are Non-redundant

What information might these population bursts and the rank of neuronal spiking contained therein represent? Given the possibility that neuronal sequences may represent a separate code from spike rate and latency following stimulus onset, we were motivated to explicitly examine whether the sequence-based code within population bursts and the rate-based code represent distinct or overlapping information.

We first examined whether stimulus information is captured by population spike rate regardless of whether or not that neuronal population exhibits a clear burst of spiking. If rate-based coding is separable from sequence-based coding within population bursts, then information content specific to an image category should be decoded from population spike rates both within and outside of bursts. Supporting this, classifiers trained and tested separately using population spike rates when a burst is detected and outside bursting periods both provide above-chance classification accuracy for taxonomic categories using either only the sequence-related units or all units (Extended Data Fig. 6a-b).

We next investigated whether the sequence of a set of spiking units within a burst still contains stimulus information even when their spike rates are relatively controlled across stimulus categories. If a set of units all fire at a similar rate within a burst across different categories but with systematically varying ranks, then sequence-based information should differ from rate-based information. To test this, for each recording, we selected five sequence-related units that participated in the most bursts for all four categories, and only considered bursts where all five participated. By selecting units and bursts in this manner, the spike counts of the selected units do not significantly differentiate stimuli across categories (Repeated-measures ANOVA: $p's > 0.05$; Fig. 5a; see example raster plots in Extended Data Fig. 6c). Across recordings, sequence-based decoding accuracy in these rate-controlled units remains significantly greater than chance (true vs. shuffled in mixed-effects modeling: 28.2% ± 1.5% vs 24.4% ± 0.5%, $t(34) = 2.69$, $p = 0.011$, $r_{equivalent} = 0.42$). Thus, even when spike rate is relatively controlled within a burst, the ranks of a set of units can still distinguish the presented stimulus categories.

We then directly examined how much information about the stimulus is conveyed by each unit's spike rate and rank order within a sequence occurring during population bursts (see Fig. 5b and Extended Data Fig. 7). If a unit's spike rate and rank order carry non-redundant information about a stimulus, then knowing both the rank of a unit and how many times it spikes within a burst should provide no less information about the stimulus than the sum of the information separately associated with the unit's rank and spike count alone[34-36]. We formally estimated for each unit the information gain about the categorical information of a stimulus, s, when using its relative rank in spiking sequences alone, $I(r; s)$, when using the spike count alone, $I(c; s)$, and when using both, $I(c, r; s)$. Consistent with our selection of sequence-related units, the rank order of units with reliable ranks for at least one stimulus category captures more information about the stimulus as compared with the less reliable, non-sequence-related units (Extended Data Fig. 8a). Both types of units, however, do not differ significantly in the amount of information captured by their spike counts within bursts (Extended Data Fig. 8b). Critically, the sum of information solely related to the rank

or spike count is smaller than the information gain when both rank and spike count are considered together – $I(c; s) + I(r; s) < I(c, r; s)$ – in most recorded units (Extended Data Fig. 8c). This interaction information, namely $I(c, r; s) - I(c; s) - I(r; s)$, is significantly greater than 0 across recordings for sequence-related units (random-effect at the recording level: $t(17) = 4.52$, $p = 3.01e^{-4}$, $r_{equivalent} = 0.74$, $n = 18$ recordings) and accounts for an average of about 43% of the total information conveyed by spike count and rank combined (Fig. 5b). Sequence-related units also show a significantly greater interaction information captured by spike count and rank as compared with non-sequence-related units (Extended Data Fig. 8c). Together, these results suggest that information about a unit's rank and spike count within a sequence synergistically provides non-redundant information to support visual categorization, particularly among units with a reliable sequence rank across bursts.

We next examined how non-redundant rank- and rate-based information may coexist within a sequence. Previous research suggests two possibilities: units sensitive to rate-based coding could spike either earlier[10] or later[6,37] in a neuronal sequence. To test these possibilities, we assessed the extent to which each unit's relative rank is related to its spike rate decoding of category-specific information. Across recordings and stimulus categories, we observed that sequence-related units tend to contribute to the population rate code earlier in the neuronal sequence for a given stimulus category. However, such a pattern does not hold for non-sequence-related units (Extended Data Fig. 9).

The presence of two complementary neural codes raises the question as to the relative importance of spike rate and rank order in representing stimulus information. One possibility is that the benefit of information coding based on spike order may become more apparent as the number of neurons increases[11,38]. To examine this, for each recording session, we randomly selected subsets of sequence-related units (5-95%, in increments of 10%), and recomputed our decoding accuracies separately using spike rate across the task period and then spike sequence within population bursts. In both cases, decoding accuracy increases as we include more neuronal units (see Fig. 5c for an example and group average). Critically, although decoding accuracy is initially higher with fewer units when using spike rate compared to using spike sequence within bursts, decoding accuracy increases more rapidly when using spike sequences as the number of included units increases (also see Extended Data Fig. 10). These results suggest that rank-based coding may become more apparent as recordings from larger populations of neurons become available[38].

Discussion

Our data demonstrate that populations of neurons in the human ATL exhibit discrete bursts of spiking activity organized into precise temporal sequences. These neuronal sequences convey higher-order visual information across a hierarchy of categories and exemplars as participants complete a visual categorization task. This sequence-based code complements and is not redundant with the conventional neural codes based on spike rate or latency following stimulus onset[1-5]. By leveraging the opportunity to examine spiking activity from a relatively large population of neurons in the awake human brain, these findings provide empirical support for early theoretical models positing the presence of complementary coding schemes in the human brain[9,10,15].

These results highlight the role of neuronal sequences in human cognition. While previous research based on animal models has identified similar physiological signatures in primary sensory cortices[6,17], our data reveal a comparable coding principle in the human ATL, emphasizing the role of neuronal sequences in information coding across species. Notably, these neuronal sequences within spiking bursts occur on a compressed timescale (e.g, 50-150 ms). Consequently, they differ fundamentally from sequential neuronal activity elicited by time-evolving environmental inputs[18-21] and from sequences that occur over longer timescales[39]. These findings align more closely with the rapid replay of neuronal sequences in the context of memory, as previously reported in animal models[40] and in the human neocortex[25]. Yet, in contrast to these prior studies in which the replay of neuronal sequences is explicitly linked with memory retrieval, our current task does not involve an explicit memory load[25,40]. These data thus suggest that neuronal sequences within population bursts may play a more general role in representing information in the human neocortex.

The neuronal sequences we identify occur within transient and discrete bursts of population spiking activity. These bursts, containing such sequences, represent discrete population events that appear to arise uniformly throughout a trial, regardless of stimulus category. Because we are recording from the higher-order association cortex, these bursts may differ from sensory-driven activity in lower-level regions. For instance, the detected bursts often coincide with cortical 80-120Hz ripples in the association cortex[26], which may be related to information processing and communication in the human neocortex[41-44]. While it is possible that these bursts are related to eye movements and visual fixation on the target stimulus, the bursts' distributed timing throughout the trial period, extending up to one second following stimulus onset, makes this unlikely. Moreover, such a gaze-dependent explanation would be inconsistent with the clear timing of stimulus-locked classification accuracy observed when analyzing the spike rate responses (Fig. 3b and Extended Data Fig. 4b-c). In addition, prior evidence has shown that even within sensory cortices, bursts of sequential neuronal activity in the absence of sensory stimulation may still contribute to information processing[6,45]. The spiking bursts we observe here may reflect similar internal processing of information, a question that requires further investigation (see also Supplementary Discussion).

Importantly, the neuronal sequences we observe during spiking bursts are not redundant with or simply a consequence of the spike rate response or spike latency following stimulus onset. Neural coding based on population spike rate and average latency following stimulus onset appears robust and independent of whether activity is examined within or outside these spiking bursts. Thus, the information conveyed by these conventional neural codes is dissociable from that captured by the relative rank of neuronal firing within spiking bursts. Conversely, sequence-based coding within the bursts remains robust even when controlling for spiking rate. Formally analyzing the information contained within these spiking bursts reveals greater information conveyed by the combination of spike count and relative rank of the units as compared with using either measure alone. Although fast neuronal sequences have been linked with memory replay of prior experiences[25,40], the rank order of firing within these bursts are not simply recapitulating, or replaying, the order of spike latencies following stimulus onset. Thus, the neuronal sequences within these discrete spiking bursts

may represent a complementary and synergistic neural code, alongside spike rate, for high-level visual representation in the human brain.

Why might the human brain employ multiple codes to represent information? One potential key advantage neuronal sequences, relative to a rate-based code, is their computational efficiency[9-12]. By using the temporal order of spiking rather than the number of spikes, sequences can capture complex information with relatively sparse spiking activity[11]. This contrasts with the coding scheme implemented in many contemporary advanced artificial intelligence systems[11]. One proposed mechanism for information coding based on neuronal sequences is that a series of spikes may progressively activate a set of synapses along an apical dendrite, modulating the activation level of a post-synaptic neuron depending on the spiking order of pre-synaptic neurons. This would position the dendrite as a focal site for neural computation[11,46,47]. The role of this neural code based on neuronal sequences may become more apparent as recording technologies improve our ability to capture spiking activity across larger populations of neurons[38].

Previous studies have shown that neuronal sequences are often limited to a set of pre-existing templates constrained by underlying neuronal connections that can bias the order of neuronal spiking in a novel environment or for a novel stimulus[6]. We similarly find a set of template sequences that encode information across a representation hierarchy. These template sequences rely on the activity of a subset of units that we label as sequence-related units, each exhibiting a relatively constrained rank position within each category. These templates may reflect pre-existing neuronal connections[6,27], in which case every individual template sequence reflects initial stimulus-dependent activation of a different set of units which consequently leads to a stereotyped sequential activation of connected neurons. Alternatively, the template sequences may reflect connections formed during the experiment. Our data cannot distinguish these possibilities as participants had completed hundreds of practice trials before recording.

In sum, our data demonstrate that neuronal sequences within discrete bursts of spiking contribute to the representation of higher-level visual information in humans. Contemporary models often abstract away information contained within spike timing and instead rely on Poisson-based spike rates to capture the relationship between brain activity and behavior[48-50]. However, evidence has suggested that neuronal activity is not Poisson-like[51,52]. For example, population spiking activity across a group of neurons can often manifest as bursts during a task or at rest[7]. Moreover, temporal features of spiking activity[2], such as exact relative spike timing[53], latency[54], and synchrony[55], may also contribute to information coding. Our data add to this literature by demonstrating that neuronal sequences within bursts of population spiking convey non-redundant information about visual categories and exemplars relative to spike rate. These findings underscore the broader role that the temporal order of spiking activity across a population of neurons can play in human cognition.

Methods

Participants

Eight right-handed participants (36.25 ± 3.38 years old, 3 females, IQ: 86.50 ± 5.35; see Supplementary Table S1) with drug-resistant epilepsy underwent a surgical procedure for placement of intracranial electrodes for monitoring of potential epileptogenic regions using platinum electrode contacts (PMT Corporation, Chanhassen, MN, USA) implanted subdurally on the cortical surface and/or deep within the brain parenchyma (stereo EEG). Pre-surgical evaluations of each participant suggested a potential seizure onset zone in the temporal lobe areas. As such, in each participant, we placed two 64-channel microelectrode arrays (MEA; 3.2 mm × 3.2 mm, Cereplex SI; Blackrock Microsystems, NeuroPort Central Suite v 7.0.3.0, Salt Lake City, UT, USA) in the middle temporal gyrus of the ATL, approximately 1-2 cm apart from one another and approximately 2-4 cm from the temporal pole (Fig. 1b).The implant site was selected to fall within the expected resection area where no structural abnormalities were identified based on pre-operative MRI and visual inspection during the implant surgery. Of the eight participants, five received a surgical resection that included the tissue where the MEAs were implanted. For the remaining three participants, one received a surgical resection that involved regions posterior to the implanted MEA in the temporal lobe and had a noticeable improvement in their seizures following surgery. One had bi-temporal lobe seizures and received a Responsive Neurostimulator Device (RNS) in the bilateral hippocampi and subsequently had a significant improvement in their seizures following surgery. The third participant did not have seizure activity captured during the monitoring period to suggest a safe and effective surgical resection and did not experience any change in seizure frequency or cognitive functions (e.g., vision, language, or memory) following the removal of the monitoring electrodes. All participants consented to National Institutes of Health (NIH) IRB-approved research protocols (reference numbers 11-N-0051 and 15-N-0081).

All participants successfully completed a visual categorization task outlined below (see Fig. 1a and Extended Data Fig. 1a-c). However, not all implanted MEAs yielded sufficient single-unit data during the behavioral task within a given recording. Following the preprocessing and spike sorting procedures outlined in the following sections, we assessed for effective single-unit data in each experimental session and separately in each array implanted in each participant. We consider each array and each experimental session during which the participant completes the task as an independent sample. This is because the recorded units vary across arrays, and even within the same array, they tend to differ on subsequent days[23,24]. We refer to each session recorded by each array as a separate recording for subsequent analyses. Hence, if a participant performs the task once and if they have two arrays, this will generate data for two separate recordings for analysis. Similarly, if we examine the data from one array as the participant performs the task twice on two subsequent days, this will generate data for two separate recordings for analysis as well. For subsequent analyses, we required a recording to contain data from more than 10 units in an array and more than 100 bursts during the visual categorization task (see Detecting Spiking Sequences and Sequence-based Decoding for details). Based on these

thresholds, we retained 18 recordings for further analyses, which reflect data recorded across 8 participants and 12 physical arrays (see Extended Data Fig. 1e for details).

Visual Categorization Task

We asked participants to perform a visual categorization task to examine neuronal correlates of information processing across different levels of the representation hierarchy. The main component of the task involves presenting a single image on a laptop screen for 500 ms. Participants then try to categorize each image into one of four options indicated by text labels shown around the image (see Fig. 1a). Participants make their judgment by pressing one of four arrow keys corresponding to the available text labels. As accuracy is emphasized over response times, there is no time limit for the response. Once the participant makes a selection, the screen turns blank for 200 ms before the next image appears.

Based on the image content, the visual categorization task includes three major trial types. First, in trials designed to examine the representation of broader taxonomic categories, the image is chosen from and categorized into one of four taxonomic categories: ANIMAL, OBJECT, PERSON, and PLACE (Extended Data Fig. 1a). Each category includes a set of 60 unique images. Second, in trials designed to examine the representation of individual exemplars (e.g, different individuals within the PERSON category), the image is chosen from one of four famous US presidents (John F. Kennedy, William J. Clinton, George W. Bush, and Donald J. Trump; Extended Data Fig. 1b). We selected 15 unique images to include in our image set for each president. Third, to rule out the possibility that the recorded neural signals reflect motor responses rather than the information content associated with the image, we included a set of arrow trials that all but a subset of participants had completed. During these control trials, participants indicate the direction of an arrow presented as an image from one of the four possible directions (UP, DOWN, LEFT, RIGHT; Extended Data Fig. 1c). We selected a set of 15 unique images for each direction to use in our image set for arrows. In each experimental session, the images we used for each trial type were randomly drawn from the respective image sets. All images across different trial types (taxonomic, presidents, or arrows) were cropped, resized, and phase-scrambled to gently blur individual features that could be used for categorization. We balanced the image set for luminance, contrast, and spatial frequency using the SHINE toolbox[56]. Each image covers approximately 50% of a 16-inch laptop screen centered over a gray background.

In a typical session, participants begin with 1 block of 20 arrow trials, and then complete 4 blocks of 60 taxonomic trials and 1 block of 60 president trials, yielding a minimal 320 trials per run. Within each block, we presented images from that trial type in random order, with the requirement that the number of images from each category, president, or arrow direction is balanced within a block. Participants performed at least 1 practice run one to three days before their surgical implant to ensure good behavioral performance. As time permitted during intracranial recording, participants completed 1 to 4 runs per experimental session for 1 to 2 sessions, yielding a total of 951 ± 121, 245 ± 29, and 66 ± 6 trials on average for taxonomic, president, and arrow trials, respectively, with recording data (see Extended Data Fig. 1a-c for individual data). To motivate the participant, we provided feedback at the end of each block, indicating the number of correct responses (e.g., “51 of 60 correct”). To

estimate baseline neuronal activity for subsequent normalization, we also presented a noise image with scrambled pixels at the beginning and at the end of each block for 1000 ms. Participants passively viewed these noise images without any responses required.

Single-unit Recording and Analysis

We recorded and identified single units based on our previously reported approach[23-25]. In brief, each MEA is organized into an 8 × 8 grid of micro-electrodes, with each electrode spaced 400 μm apart and extending 1 mm into the cortical surface. We digitally recorded signals at 30 kHz using a Cerebus acquisition system (Blackrock Microsystems), with 16-bit precision and a range of ±8 mV. To extract single-unit spiking activity, we referenced the activity of each electrode of an array to the average of all electrodes on that array. We then bandpassed (0.3 to 3 kHz) time series of each channel, one at a time, into the Plexon Offline Sorter (Plexon, Inc.; TX) for manual spike sorting[23,24]. In this procedure, we converted the continuous-voltage time series into a population of voltage snippets (1.07 ms long, 30 samples) that crossed a manually defined voltage threshold. We set an individual threshold for each channel such that random noise fluctuations in the signal would occasionally cross the threshold and be captured as a noise snippet. We projected each snippet into principal component space and manually drew a boundary around clusters of waveforms that were separable from each other and from noise throughout the duration of the experiment. In this manner, we identified a total of 2110 putative single units in the current dataset (117 ± 13 units per recording).

As units recorded from different arrays or from different experimental sessions on subsequent days can exhibit variations, we treat each recording as a separate sample, but their dependency could not be fully excluded. To account for the multi-level data structure (see Statistics and Reproducibility), we therefore employ a mixed-effects modeling approach to assess the effects of interest, allowing for generalization across different recordings while accounting for variances at the participant, session, and array levels (see Extended Data Fig. 1e). We also quantified the quality of each identified unit by calculating signal-to-noise ratio (SNR) and a normalized isolation score (from 0 to 1) to capture the consistency of a unit's waveform across spikes and how well a unit's waveform can be separated from the waveforms of other units and noise snippets[57] (see Extended Data Fig. 1f). Across participants, the mean SNR for all identified units is 1.98 ± 0.06 (median = 1.99) and the mean isolation score for all identified units is 0.94 ± 0.01 (median = 0.95). The average baseline spike rate across all units is 1.15 ± 0.27 Hz (median = 1.04 Hz, log spike rate≈ 0). These metrics are on par with prior Blackrock Utah array data acquired under a similar recording settings across different tasks[24,25].

Detecting Spike Sequences

When examining the population spike raster during the behavioral task, we observed several clear bursts of coordinated spiking activity in which groups of recorded units fire close in time (within ~50 to 150 ms; Fig. 1c). As groups of neurons that are active during bursts usually are not perfectly synchronized, we were motivated to investigate whether the neurons in a population fire in a specific temporal order and whether patterns of sequential spiking contain information about the presented stimulus.

To do this, we first have to identify when bursts of spiking activity occur. We based the detection of these individual bursts on transient increases in the number of spiking units. Two parameters could influence the detection of such bursts: the Gaussian kernel size used to calculate the instantaneous spike rate (i.e., the smoothing factor) and the minimal number of units recruited within a burst (i.e., the prominence threshold). The ideal settings for these parameters depend on the number of recorded units and the spike rate of those units, both of which would be different for each recording. Therefore, no single set of parameter values would be able to reliably capture bursts that were evident during visual inspection. To identify bursts while minimizing false discovery, for each experimental session, we parametrically varied these factors to determine the reasonable detection thresholds to control for the false positive rate. For each recording, we generated a surrogate time series of spike times for each unit using a Poisson process governed by the firing rate of the unit in the original data (Extended Data Fig. 2a-b). We then selected the detection parameters such that, within each recording, the number of detected bursts in the real dataset was at least 10 times greater than the number of bursts in the surrogate dataset with the same parameter settings, thus controlling for the false positive burst detection rate to be less than 10% (Extended Data Fig. 2c, g). Across recordings, these false-positive-controlled parameters only reside in a limited range in a broader parameter space, suggesting some homogeneity in bursting activity across participants/sessions/arrays (Extended Data Fig. 2d). For example, although burst activity may be correlated to the number of total units detected, it does not vary based on a unit's spike rate or the number of trials tested (Extended Data Fig. 2f). Ultimately, we identified 18 recordings that contain at least 100 bursts during the taxonomic trials for subsequent analyses (mean = 2504 ± 590 bursts per recording; median = 1238 bursts; range = 360 to 7559 bursts; burst rate = 0.99 ± 0.19 Hz).

After identifying each burst in each recording, we then extracted a normalized rank order of the units within that burst. Because spike time and order are highly correlated within a burst sequence[58], the order information based on a unit's mean or peak spiking time can serve as a proxy for the temporal order of unit activity within a sequence while minimizing potential measurement noise of spike timing at the single spike level[9,28]. We therefore estimated a unit's spike rank within a burst based on the center of mass of the peak instantaneous rate for that unit in the burst[27,28]. We scaled these rank values from 0 for the earliest unit in the sequence to +1 for the latest unit in the sequence[27]. If a unit does not participate in a burst, it was not assigned a rank for that burst. We used these normalized rank values in our subsequent analyses.

Sequence-based Decoding

We developed classifiers to decode visual information content based on the sequence of spiking activity within each burst using a template-matching approach[30,59]. In brief, in a set of training data, we created templates of spike sequences averaged across bursts evoked by images within a given category (taxonomic categories, presidents, or arrows) and then used those templates to test the categorization of spiking sequences in an independent held-out set of bursts. Building a classifier in this manner required several key steps.

First, we reasoned that a minimum requirement for burst sequences to code information would be that two or more units within the population have reliable ranks for the different image categories based on their average firing time within a burst. Units could have unreliable sequence positions for various reasons. For example, units with poor isolation during spike sorting could manifest as more variability in spike timing, and some units may not contribute to sequence coding at all. Units with unreliable sequence positions would likely reduce the sensitivity of a population sequence decoder. We therefore excluded these units from the category-specific templates used for classification. This feature selection step is analogous to using a regularization technique to suppress non-predictive weights in standard classifiers[60].

To identify these reliable units, we created surrogate datasets for each session by randomly shuffling the ranks of the units contributing to each individual burst 2000 times. We identified units with reliable ranks separately for each taxonomic category by comparing the mean and standard deviation of ranks observed across all bursts from a given category to surrogate distributions of these values (see Extended Data Fig. 3a). We retained a unit as long as the mean or standard deviation of the observed normalized rank across bursts significantly deviate from the surrogate distribution in at least one taxonomic category (alpha = .05, two-tailed for mean-related tests and one-tailed for variance-related tests; see the right panel in Extended Data Fig. 3a). Because this unit selection step is omnibus and is separately applied to each category, it imposes minimal assumptions for the specific relationship between a unit's rank and the stimulus categories. In the end, all 18 recordings we retained for subsequent classification analysis have at least 10 units across at least 100 bursts meeting this requirement in taxonomic trials (mean ± s.e.m. = 67 ± 11 units; median = 60; range 11-159 units). This set of sequence-related units accounts for 52.6% ± 4.8% total units recorded and sorted for taxonomic classification (see Extended Data Fig. 3b).

A second requirement for building a classifier capable of sequence-based decoding is that the independent templates from the same category have similar sequences, while templates from different categories have different sequences. To verify this, in each recording, we created five independent template sequences for each category by averaging the normalized ranks of 20% of the bursts randomly selected without replacement from trials in which a stimulus from that category was presented. Only units with reliable sequence positions were used in these template sequences. We then evaluated the similarity between any category template sequences by computing the rank-order correlation between them (Kendall's τ). As illustrated in the data from an example recording (Fig. 2b), we ranked the average sequence order for a given category in one fold of data based on the sequence order evoked by images from the same category averaged across non-overlapping folds of data (hence, within-category sequence similarity) or based on the sequence order evoked by images from another category (hence, between-category sequence similarity). We calculated the average Fisher's transformed Kendall's τ as a measure for the similarity between any within- or between-category template sequences. We contrasted these similarity measures for within- and between- category template sequences, namely the difference between the diagonal and off-diagonal values of the similarity matrix after factoring out participant-, session-, and

array-level variances, to verify if this second requirement was satisfied (see Extended Data Fig. 3c).

Finally, having identified the reliable units with ranks that could be used to carry stimulus information, and having verified that the rank ordering of these units is consistent within categories and different across categories, we built our classifier. Using only the units with reliable ranks that spiked in at least 2 bursts per stimulus category and the bursts that contained spikes from at least two such units, we created a new template sequence for each category by averaging the normalized rank order of all bursts aggregated from a training set of all but one burst (i.e., leave-one-out validation). We then computed Kendall's τ between the sequence of spiking activity within the held-out test burst and each category-specific template sequence. We decoded the category of the held-out test burst based on which category template sequence yielded the maximum value of Kendall's τ (see Fig. 2c), leaving bursts that yielded ties for the maximum value unscored. Classification accuracy was defined as the mean decoding accuracy across all scored bursts. To determine an empirical chance for each recording, we contrasted the original classification accuracy with the average classification accuracy obtained by repeating the above procedure 200 times after shuffling the rank order of each burst and computing leave-one-out decoding of each shuffled burst against templates created from the remaining shuffled bursts (chance performance of ~25%). To test the generalizability and specificity of this sequence-based classification, we repeated similar analyses for president and arrow trials, with relaxed requirements on the number of bursts required for these analyses to accommodate the reduced number of trials in these conditions.

Rated-based Decoding

To examine if the population spike rate of the recorded units contains information about the category of the presented image, we constructed linear classifiers using the instantaneous spike rate (200 ms sliding window, with steps of 20 ms) of the population of units in each recording during the task. We quantified neural decoding based on the population spike rate as the prediction accuracy when the model was applied to a held-out dataset.

Before the decoding analysis, we first converted the spike rate in each time window to a z-transformed, baseline-corrected spike rate by subtracting the mean and dividing by the standard deviation of the square root spike counts during the baseline period when a noise image was presented on the screen[61]. We then used a linear logistic regression classifier model with early stopping[62] to predict image category from population spiking activity. In this model, we used trials in which the participant correctly identified the image category, and implemented a 20-fold cross-validation procedure to estimate classification accuracy (see Extended Data Fig. 4a). Each held-out set consisted of approximately 5% of all trials uniformly distributed across the session. For each fold, we randomly selected one quarter of the training trials to be used as the early stopping test set. To avoid overfitting, we iteratively evaluated this test set to determine when to stop annealing the regression weights[62]. We repeated the random selection of early stopping trials 50 times per fold, and computed the average resultant weights for each fold before computing prediction accuracy on the held-out set. We separately performed this procedure using the instantaneous rate of the

units in each time window from −250 ms to 1750 ms following stimulus onset to visualize the time course of image category discriminability (see Extended Data Fig. 4b-c). In this case, the number of predictors used for classification at each time point is therefore equal to the number of units. Based on the same approach, we also built a single classifier that estimated overall classification accuracy for the entire response period aggregating multiple 200ms windows of normalized instantaneous rate that spanned from 100 ms to 1400 ms following stimulus onset. In this case, the total number of predictors used for classification is therefore the number of neuronal units multiplied by the selected time windows. Here, we chose a wide time window (100 to 1400 ms) based on the aggregate distribution of response times to capture stimulus-related neural responses with minimal analytical assumption. Both separately for each time window and for the aggregated data across time windows, we obtained an empirical chance-level classification accuracy based on data trained and tested using shuffled trial labels. We used the same procedures to estimate the overall classification accuracy for taxonomic trials, president trials, and arrow trials separately. With higher trial counts for taxonomic trials, we also estimated classification accuracy separately for each individual category.

Unit Contribution to Rate-based Decoding

To determine the extent to which each unit contributes to the rate-based code at the population level for each taxonomic category irrespective of time, we quantified the relative contribution of each unit to overall population rate-based classification accuracy using a leave-one-out procedure[63]. Specifically, based on data from all task-relevant time windows (100 to 1400 ms after stimulus onset), we iteratively excluded one unit at a time and recomputed the overall classification performance, which was quantified as d' in the decoding accuracy between true versus shuffled data across the 20 folds of classification (see Extended Data Fig. 9a). Excluding a unit, u, in this manner generates a measure of the relative contribution, Cr, of that unit to the overall classification accuracy:

$$Cr = d'_{all} - d'_{all-u}$$

where d'_{all} is the overall classification performance using all units (true vs. shuffled data), and $d'_{all-u}$is the classification performance after excluding that unit, u. The greater the Cr, the more decoding accuracy decreases after the exclusion of a unit, hence suggesting the importance of this unit to rate-based information coding. We normalized these contributions by scaling these values within each recording from 0 to 1:

$$\widetilde{Cr} = \frac{Cr - Cr_{min}}{Cr_{max} - Cr_{min}}$$

which generates an empirical, scaled contribution metric, $\widetilde{Cr}$, in which 0 indicates the least and 1 indicates the most contribution of a unit's spike rate to the overall classification performance at the population level. A similar leave-one-out approach, however, would not be appropriate for estimating a unit's contribution to the sequence-based information code, since omitting a unit may affect not only the test sequence but also the template sequences obtained from the independent training data.

Sequence- and Rate-based Information

To determine whether sequence- and rate-based codes represent distinct or overlapping information, we employed several methods to assess the relative independence of these codes for encoding stimulus information. We specifically focused on taxonomic trials, which constitute a greater number of trials per participant and thus offer a more robust evaluation of the relationship between sequence- and rate-based neural codes.

First, to test whether rate-based classification is robust both within and outside of bursts, we performed decoding analyses for taxonomic trials as outlined above based on data aggregated from task-related time windows where at least one burst was identified and separately from time windows in which no bursts were found (see Extended Data Fig. 6a). We examined whether classification accuracy is significantly greater than chance in both conditions, irrespective of whether or not populations of neurons exhibit a transient increase in bursting activity.

Second, to test whether sequence-based information is retained even when spike rates could not significantly distinguish different stimulus categories, we selected the top five sequence-related units that had participated in the most bursts of the four taxonomic categories, and only considered the bursts when all five selected units participated. Selecting five units ensures that a reasonable number of bursts can be identified per recording, while also reducing the variability in the measure of rank-order similarity as compared with including only two or three data points. On average, the chosen bursts account for 10.2% ± 1.9% of total bursts across participants, in which the five selected units fire at least once within a burst in each one of the four categories. As these units participate in bursts in response to images from all categories, spike rates therefore are less discriminative across stimulus categories (see Fig. 5a for group average and Extended Data Fig. 6b for individual raster examples). Using the ranks of only these selected units, we then attempted to decode the visual categorical information using a similar sequence-based classifier as described above. Briefly, we considered the ~10% chosen bursts as the held-out test data and all the remaining ~90% bursts as training data. As the selected units do not simultaneously participate in all of the training bursts, we took the mean of their normalized ranks across these training bursts to create category-specific templates using these five units. We then compared the ranks of these five selected units in the held-out test data with the category-specific template sequences constructed from the training set, and retained the category with the highest rank-order similarity as the decoded outcome (Fig. 5a). We then compared the overall decoding accuracy relative to the empirical chance level (~25 %) established by shuffled rank data of the test sequences 1000 times.

Third, to formally quantify the information content contained in spiking sequences, we examined how much information a unit's spike count and its rank within a sequence contains about the presented images in the taxonomic trials. Spiking sequences could potentially contain information about a stimulus in several forms: the number of times that a unit spiked and the temporal order or rank of these spikes within a sequence[9,10]. The information content related to different stimuli, s, in an individual neuron's spiking activity, x, can be calculated as follows:

$$I(x;s) = \sum_{x,s} P(x,s) log_2(\frac{P(x,s)}{P(x)P(s)})$$

where x can be either the unit's spike count, c, or its rank, r, within a sequence. Specifying x would thus lead to formal quantification of information about the stimulus by knowing either a unit's spike count or its rank within a sequence alone, namely $I(c;s)$ or $I(r;s)$, respectively. To empirically compute these conditional probabilities and estimates of information for each unit, we constructed a contingency table capturing the frequency of a unit's rank across all identified sequences during the critical time window of the task after stimulus onset but before each trial-specific response time separately for each stimulus category (see an example in Extended Data Fig. 7). Because the spike count of a unit is sparse within a burst sequence, we binned the spike count data into 3 bins, namely 0, 1, and >1, corresponding to when a unit exhibits no spiking, spikes just once, and spikes more than once, respectively, within a burst sequence. We similarly grouped a unit's rank within a sequence into 3 equally spaced bins, capturing the early, middle, and late time periods within each burst. When a unit did not participate in a sequence (count = 0), we assigned its rank in these cases to be equally distributed across different rank bins, rendering the mutual information between rank and stimulus strictly 0, namely $I^{c=0}(r;s) = 0$. Considering that $I(r;s) = I^{c=0}(r;s) + I^{c>0}(r;s)$, the amount of stimulus information by knowing a unit's rank within a sequence is therefore only driven by the cases where a unit participates in a sequence with a least one spike.

A key issue in determining how much information is captured by either a unit's rank or its spike count is how much more information about the stimulus is available by knowing both a unit's count and rank within a sequence, namely $I(c,r;s)$, beyond knowing only its count and rank alone[34-36],

$$II(c;r;s) = I(c,r;s) - I(c;s) - I(r;s)$$

in which,

$$I(c,r;s) = \sum_{c,r,s} P(c,r,s) log_2(\frac{P(c,r,s)}{P(c,r)P(s)})$$

Here, the information gained about a stimulus by knowing both the count and rank of a unit within a sequence, namely $II(c;r;s)$, reflects the interaction between different forms of a unit's spiking activity and the presented stimulus[34-36]. If this information gain is positive, it indicates the presence of stimulus information that is only jointly represented by a unit's count and rank, suggesting non-redundancy or synergy of these two types of coding schemes in predicting the information content of a stimulus. However, if this information is negative, then at least some information about the stimulus disclosed by a unit's spike count and rank is redundant[34-36]. We quantified these metrics to examine the extent to which a unit's count and rank within a sequence provided non-redundant information about the stimuli.

Finally, as non-redundancy does not imply the lack of association between sequence- and rate-based information, we further investigate the relationship between a unit's rank in category-specific spiking and its spiking rate response to separate categories. Using the binned rank data within a sequence as described above (i.e., early, middle, and late), we examined the extent to which a unit's category-specific rank is related to its category-specific relative contribution, $\widetilde{Cr}$, to rate-based information, calculated as described above using a leave-one-out approach. This analysis may address whether units that carry more rate-based information spike earlier[10] or later[6] within a burst sequence. To achieve this, we used repeated-measures correlation[64,65] to quantify these associations within participants.

Statistics and Reproducibility

We applied a linear mixed-effect modeling approach to take into account variance within and across participants, sessions, and arrays in statistical inference[66]. Within each participant, we considered the single-unit data collected across different MEAs or different experimental sessions as independent, given that units collected by the MEAs tend to vary across recording regions and sessions[23,24]. Across participants, we pooled the data together while factoring in the nested data structure within each participant. That is, for each outcome variable Y, we modeled its means across different comparison conditions (e.g., decoding accuracy with the true or shuffled condition labels) in the following linear mixed-effects model,

$$Y \sim 1 + Condition + (1 \mid Participant) + (1 \mid Session) + (1 \mid Array) + (1 \mid Participant{:}Session{:}Array)$$

As we repeated the experiment with 8 participants across 13 sessions using different MEAs, we generated 18 recordings containing independent single-unit datasets (see Extended Data Fig. 1e). Notably, all 18 recordings exhibited above-chance decoding for taxonomic categories using neuronal sequences, while 17 out of 18 recordings showed above-chance decoding for taxonomic categories using spike rates. Regarding the decoding of exemplars within the PERSON category, 12 out of 18 recordings demonstrated above-chance decoding using neuronal sequences, and 14 out of 18 recordings showed above-chance decoding using population spike rates.

To evaluate these effects, we report the t statistic and degrees of freedom (df = #observations - #parameters) for the effect across experimental conditions after partialling out across-participant variations using the *fitlme* function in Matlab (MathWorks, Naticks, MA). All p-values from these tests are two-tailed. For time-series data analyses, we correct for multiple comparisons using a cluster-based procedure with an alpha level set at .05. We estimate the size of these fixed effects based on an equivalent measure of correlational strength, namely $r_{equivalent}$[67,68].

$$r_{equivalent} = \sqrt{\frac{t^2}{t^2 + df}}$$

Extended Data

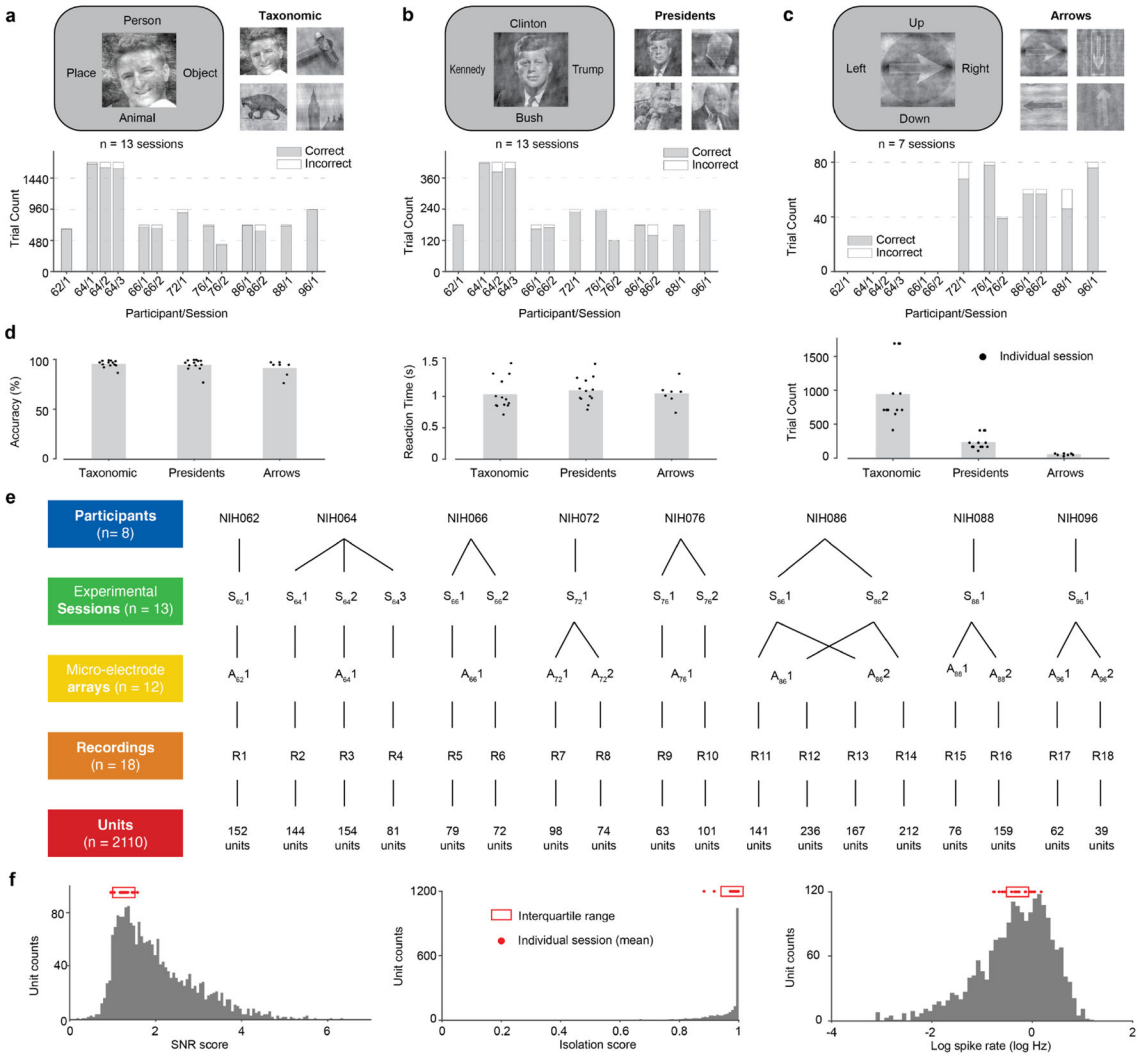

Extended Data Figure 1. Behavioral task details, data structure in the current study, and unit quality metrics.

a, An example trial using images from the four predefined taxonomic categories (*top* panel) along with trial counts for each participant in each experimental session (*bottom* panel). **b** An example trial using images of four selected U.S. presidents (as PERSON exemplars) along with trial counts for each participant in each experimental session. **c**, An example trial using images representing four arrow directions along with trial counts for each participant in each experimental session. **d**, Average trial counts, accuracy, and response times for each trial type. **e**, Across 8 participants with recordings providing meaningful unit data, we identified 18 unique recordings from 13 experimental sessions across 12 physical arrays. As units recorded from different arrays or from different experimental sessions on subsequent days can exhibit variations, we treat each recording as a separate sample. In total, we identified 2110 putative single units across the 18 recordings. To account for the multi-level data structure in our statistical analysis, we employ a mixed-effects modeling approach to

assess the effects of interest, allowing for generalization across different recordings while accounting for variances at the participant, session, and array levels. **f**, We quantified the quality of each identified unit by calculating signal-to-noise ratio (SNR) and a normalized isolation score (from 0 to 1) to capture the consistency of a unit's waveform across spikes and how well a unit's waveform can be separated from the waveforms of other units and noise snippets 60. Across participants, the mean SNR for all identified units is 1.98 ± 0.06 (median = 1.99) and the mean isolation score for all identified units is 0.94 ± 0.01 (median = 0.95). The average spike rate is around 1 Hz (log spike rate around 0).

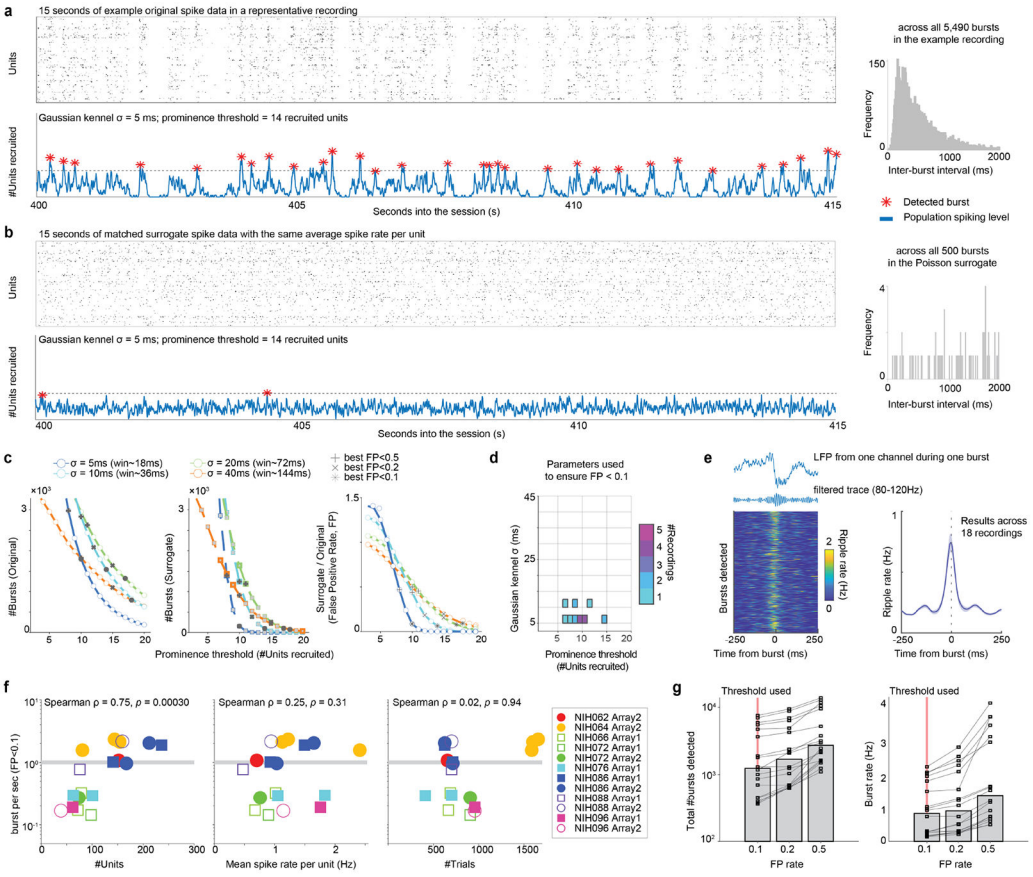

Extended Data Figure 2. Burst detection.

a, Spike data extracted from an example recording, along with the detected bursts, based on individual smoothing and thresholding parameters identified to ensure a false positive (FP) rate smaller than 0.1 as compared with surrogate data. The inter-burst intervals appear to be non-uniformly distributed. **b**, Surrogate spike data generated by a Poisson process to maintain the same average spike rate per unit over time, along with the detected bursts using the same smoothing and thresholding parameters. The inter-burst intervals in this surrogate data appear to be uniformly distributed. **c**, Systematic variation of the smoothing and thresholding parameters for each individual recording to identify the parameter set that results in a low FP rate, quantified as the ratio of detected bursts between the surrogate and the original data. **d**, The best parameter sets across recordings fall within a narrow range, indicating some homogeneity in bursting behavior across recordings. Color values

represent the number of recordings. **e**, Spiking bursts coincide with an increase in 80-120 Hz ripple rate recorded from the same micro-electrodes, observable at the level of individual bursts (*left*) and across recordings (*right*). Error areas represent the s.e.m. **f**, The number of detected bursts tends to covary with the number of total available units (Spearman ρ = 0.75, $p = 0.00030$). However, it does not depend on the average spike rate (Spearman ρ = 0.25, $p = 0.31$) or the number of included trials (Spearman ρ = 0.02, $p = 0.94$). N = 18 recordings. Two-tailed uncorrected p-values were calculated based on Spearman rank-order correlation. **g**, Increasing the FP rate leads to more detected bursts. We maintained a FP rate of 0.1 in the current study. Each data point and connected line represent the results from an individual recording.

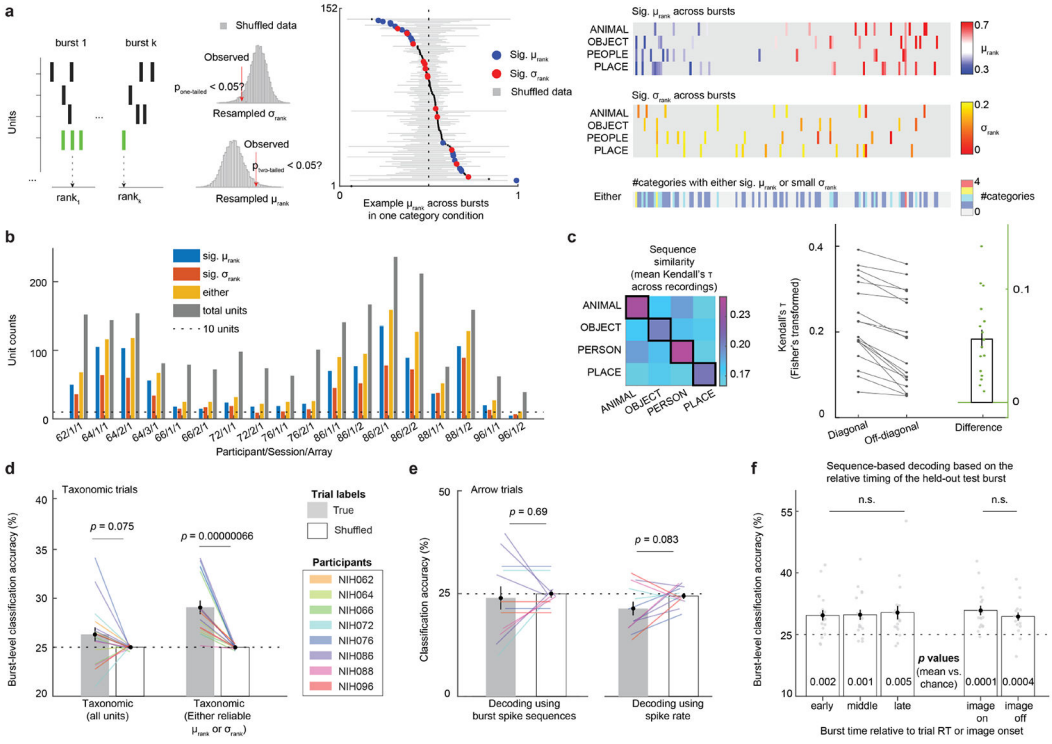

Extended Data Figure 3. Unit selection and evaluation of the sequence-based classifier.

a, To identify units that exhibit reliable ranks within bursts, we calculated the mean and standard deviation (σ) of a unit's rank across all bursts. Conceptually, units involved in sequence-based coding should demonstrate a reliable mean rank (μ_{rank}) across bursts relative to shuffled data. Units involved in sequence-based coding but with a rank consistently in the middle of a sequence may not be distinguished from the null distribution but would exhibit small variance in their rank, σ_{rank} (*left*). Hence, we considered units showing either a reliable μ_{rank} $p_{boostrap} < .05$ in either direction, two-tailed) or a small σ_{rank} ($p_{boostrap} < .05$ in the predicted direction, one-tailed) in at least one stimulus category as sequence-related units (*right*). **b**, The number of sequence-related units in each recording. Overall, sequence-related units account for 52.6% of all units. **c**, Across independent data folds, we assessed within-category sequence similarity relative to between-category sequences based on sequence-related units. Within-category sequence similarity is significantly greater

than between-category similarity across participants. **d**, Sequence-based decoding accuracy depends on unit selection. Including units with less reliable ranks decreases classification accuracy across recordings (true vs. shuffled trial labels in mixed-effect modeling: $t(34) = 1.84$, $p = 0.075$). **e**, Using spiking data from a subset of participants who completed the arrow trials, we find that neither sequence-based nor rate-based classification could reliably differentiate arrow directions. **f**, Sequence-based classification accuracy is unaffected by the timing of the held-out bursts relative to a trial's response time or to the stimulus presentation. Data are shown as the mean ± s.e.m., with results from individual recordings shown as dots and/or lines color-coded by participant. N = 18 recordings. Two-tailed uncorrected p-values were calculated using a linear mixed-effects model, accounting for participant-, session-, and array-level variances.

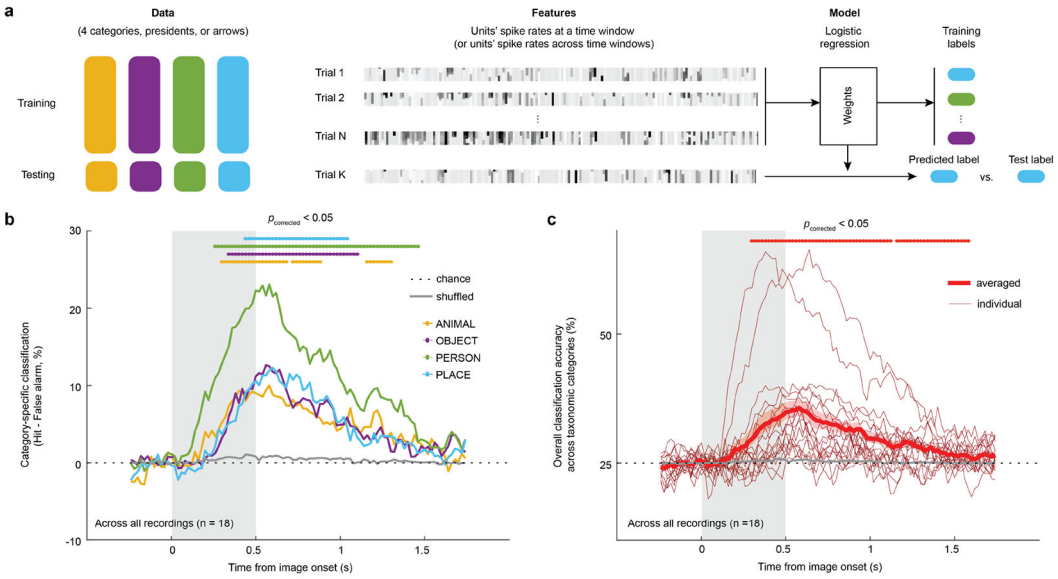

Extended Data Figure 4. Building a rate-based classifier and its performance over time.
a, For each trial type (taxonomic, presidents, or arrow), we built and tested a rate-based classifier using non-overlapping data as training and testing datasets. In each iteration, we used the training data to build the classifier using a one-vs-all logistic regression with early stopping. We then applied the training weights to the independent testing data to generate a prediction of the test stimulus label. If the predicted label is consistent with the test stimulus label, then the classification is considered accurate. We performed this analysis both using the data at each individual 200-ms time window of the task and using the aggregate spike rates data across all units within time windows from 100 to 1400 ms following stimulus onset. In the former case, the features used in the classifier are the population unit activity at a single time window with the feature length equivalent to the number of units. In the latter case, the features used are the population unit activity across time windows with the feature length equivalent to the number of units multiplied by the number of time windows. **b**, Across N = 18 recordings, a rate-based classifier can significantly decode category-specific information following stimulus onset for taxonomic categories with the classification accuracy peaking around the same time across stimulus categories. **c**, Overall classification accuracy for taxonomic categories is significantly higher than chance from 300

to 1120 ms after stimulus onset to (first cluster mean ± s.e.m.: 32.2% ± 2.0%; $p_{corrected}$ < .05). The two recordings in which decoding accuracy exceeds 50% are from participant NIH086 in two separate sessions, capturing 167 and 212 units, respectively. Thin lines indicate individual recordings and thick line group average. Cluster-based two-tailed p values are corrected at the 0.05 level.

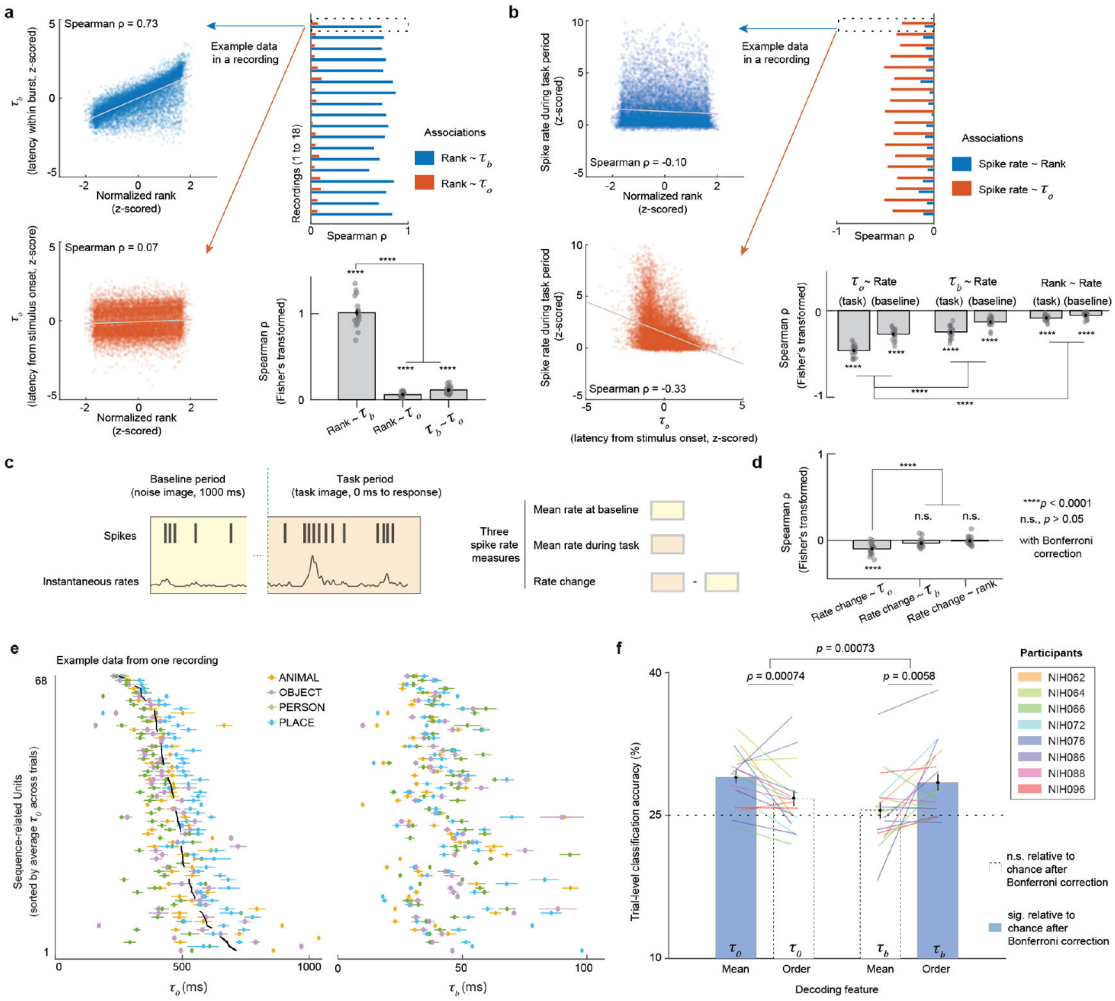

Extended Data Figure 5. Associations among spike timing measures.

a, A unit's spike rank within a burst is strongly correlated with spike latency from burst onset (τ_b, mean Spearman ρ = 0.76, range: 0.60 to 0.87), compared with spike latency from stimulus onset (τ_o, mean Spearman ρ = 0.06, range: 0.02 to 0.11). The former is over 10 times that for the latter, suggesting that rank-based measures better capture spike timing within bursts than from stimulus onset. **b**, Spike rates during both task and baseline periods are correlated with τ_o (e.g., mean Spearman ρ between task-period spike rate and τ_o = -0.43, range: −0.51 to −0.33). This relation is weaker between task-period spike rate and a unit's spike timing within bursts (rate & rank, mean Spearman ρ = −0.09, range: −0.16 to −0.02; rate & τ_b, mean Spearman ρ = −0.24, range: −0.35 to −0.11). Single-unit measures are shown as dots following z-score normalization within each burst. **c-d**, Changes

in spike rate from baseline correlate significantly with τ_o, but not with spike rank within bursts or τ_b, indicating that information conveyed by rank or τ_b differs from that by spike rate changes. **e**, In an example recording, mean τ_o across units varies by stimulus category, while the relative order of τ_o remains consistent across categories. In contrast, τ_b values are not consistent across categories, suggesting potential for information coding. **f**, Mean τ_o across units provides more stimulus information than the relative order of τ_o. Conversely, the relative order of τ_b provides more information than mean τ_b. Solid blue and dashed bars indicate significant and non-significant classification accuracy relative to chance with Bonferroni correction ($p_{corrected} < .05$), respectively. Data are shown as the mean ± s.e.m., with individual data color-coded by participant. Two-tailed uncorrected p-values were calculated using a linear mixed-effects model.

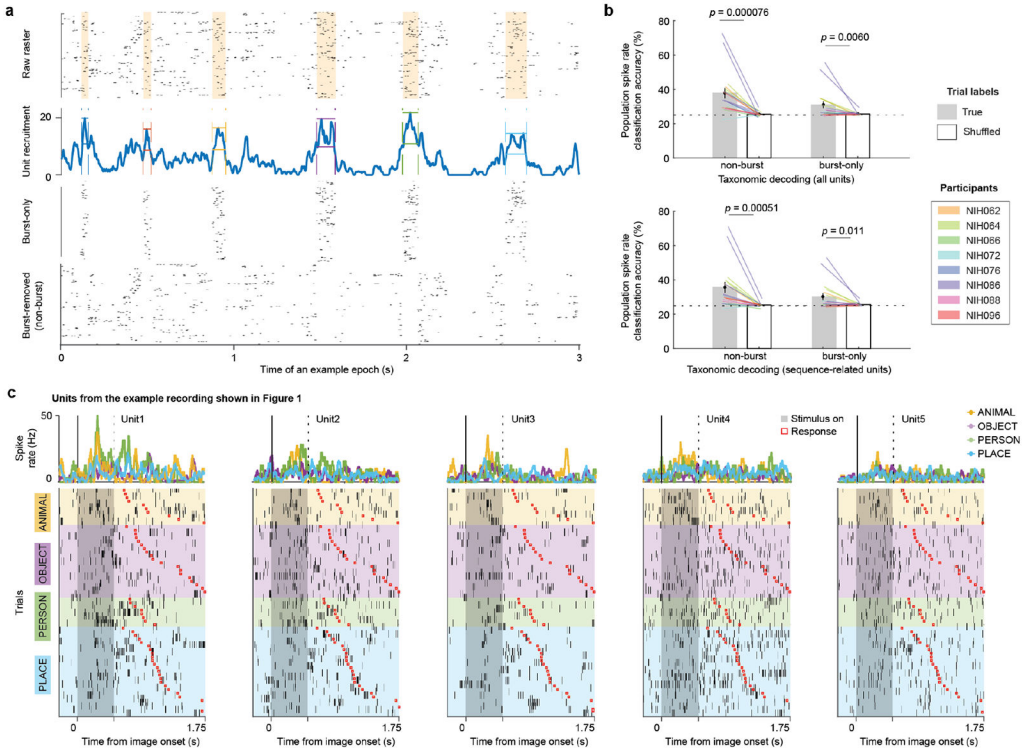

Extended Data Figure 6. Additional analyses to distinguish rate- and sequence-based information.

a, To determine if rate-based information persists across bursting and non-bursting periods, logistic regression classifiers were trained and tested based on population spike rates aggregated separately for these periods. Bursting periods, where a group of units spiked closely in time, were identified by adjusting the smoothing and thresholding parameters of population spike rate calculation for each recording, controlling the false discovery rate (see Extended Data Fig. 2). Bursting and non-bursting spike raster plots were extracted by retaining spike data within and outside bursts, respectively. Instantaneous spike rates of the population of units in these raster plots were calculated (200 ms sliding window, 90% overlap). For burst-only and burst-removed raster plots, all units and critical time windows within 100-1400 ms following stimulus onset in each trial were aggregated to

decode taxonomic categories, following the same approach as detailed in the Methods. **b**, Across recordings, population spike rate significantly distinguishes taxonomic categories better than chance using data either within or outside bursting periods, regardless of whether all units were included (mixed-effect model for burst-only: $t(34) = 4.50$, $p = 0.000076$; mixed-effect model for non-burst: $t(34) = 2.93$, $p = 0.0060$) or only sequence-related units (mixed-effect model for burst-only: $t(34) = 3.84$, $p = 0.00051$; mixed-effect model for non-burst: $t(34) = 2.71$, $p = 0.011$). Data are shown as the mean ± s.e.m., with individual recordings shown as dots and lines color-coded by participant. N=18 recordings. Two-tailed uncorrected p-values were calculated using a linear mixed-effects model, accounting for participant-, session-, and array-level variances. **c.** Example raster plots for the top five sequence-related units that spiked in bursts across all stimulus categories. These units do not significantly distinguish categories by overall spike rate, but relative rank still retains significant stimulus information(Fig. 5a).

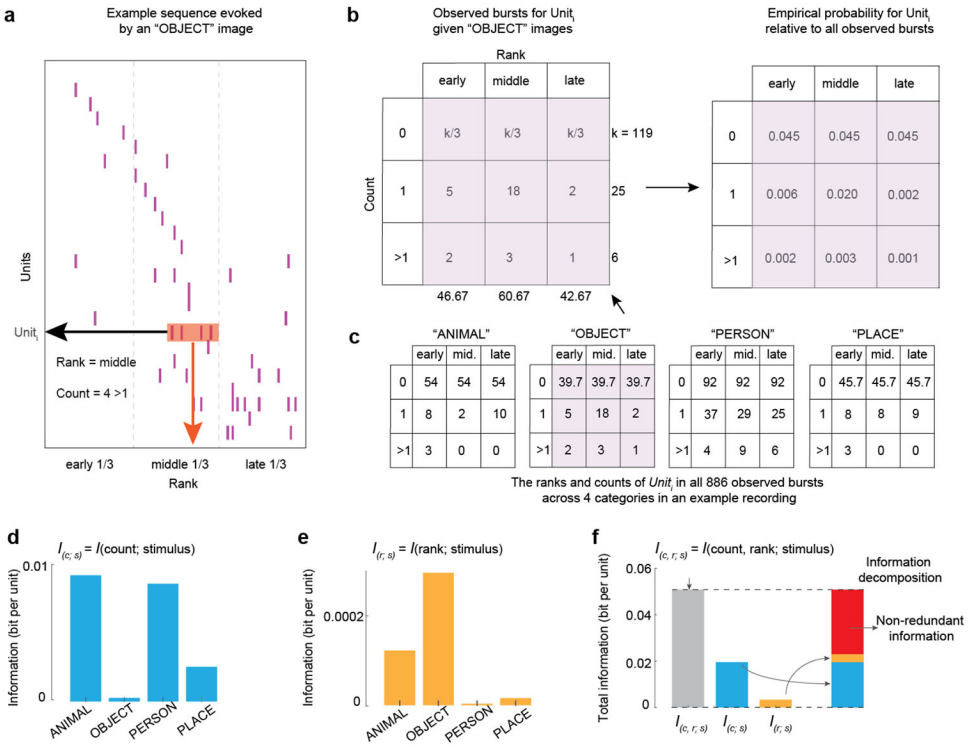

Extended Data Figure 7. Quantifying stimulus information associated with spike count and rank in burst sequences.

a, In an example burst sequence, a single unit's spiking activity can be characterized by its spike count (e.g., no spike, spiking once, or multiple times) and its relative rank within the sequence (e.g., early 1/3, middle 1/3, or late 1/3). **b**, Across burst sequences elicited by images from the same stimulus category, the unit's counts and ranks can be summarized in a frequency table (*left* panel), which can be converted into empirical probabilities relative to all observed bursts (*right* panel). **c**, Similar frequency tables can be generated for stimuli from all categories for the example unit. Using these frequency and probability tables, the empirical mutual information (*II*) between spike activity and the presented stimuli can be quantified, either based on spike count or relative rank information. **d-e**, In the example, the

spike count information for the current unit contains more information about ANIMAL and PERSON categories. In contrast, spike rank information contains more information about the OBJECT category relative to other stimulus categories. This pattern suggests that spike count and rank of the same unit may contain complementary, non-redundant information, effectively capturing different aspects of stimulus categories. **f**, Formal information theory analysis confirms this prediction, showing that the combination of spike count and rank contains more stimulus information than the sum of the information provided by spike count and rank alone (highlighted in *red*). These findings suggest a synergistic relationship between spike count and rank in representing stimulus information.

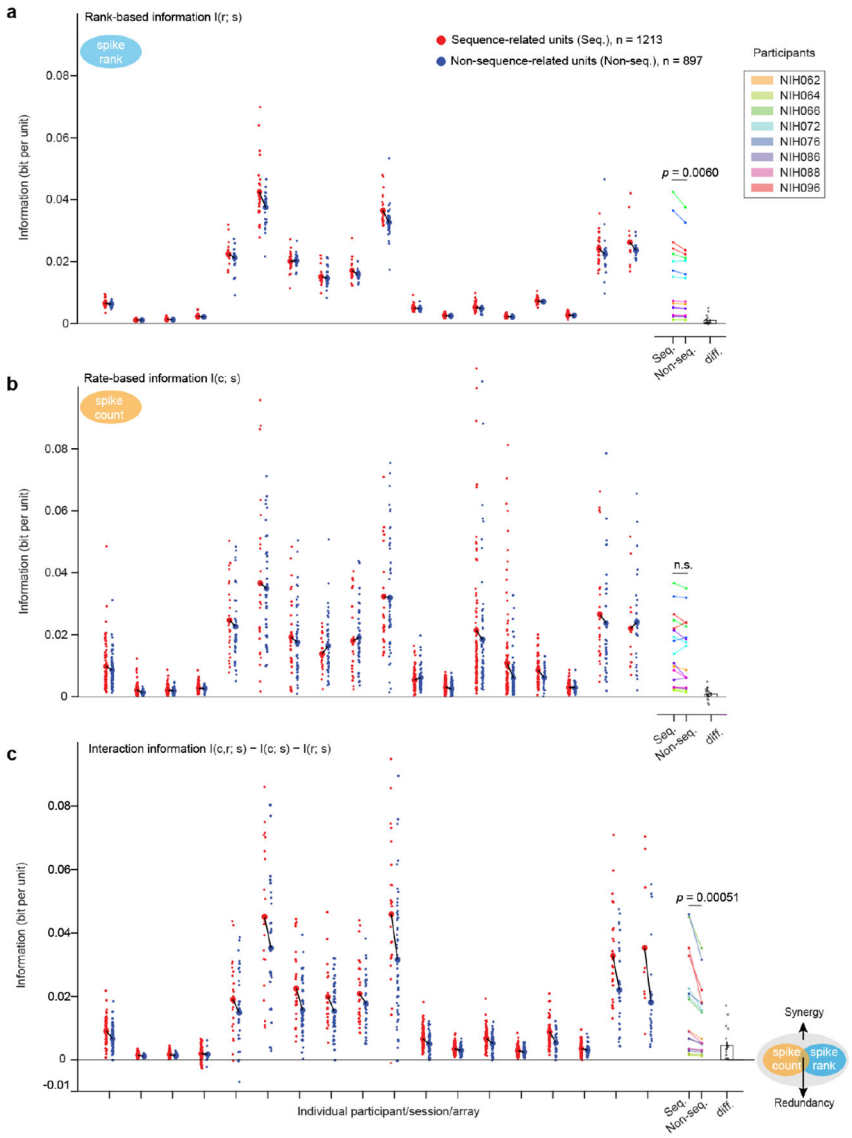

Extended Data Figure 8. Stimulus information associated with spike count and/or relative rank within bursts for each recorded unit.

a, Sequence-related units show significantly greater stimulus information disclosed by a unit's rank within a sequence, namely $I(r; s)$ as compared with non-sequence-related units

(seq. vs. non-seq. in mixed-effect modeling of $I(r;s)$: $t(34) = 2.93$, $p = 0.0060$). **b**, In contrast, stimulus information disclosed by spike count within a burst sequence, namely "($; &), is not significantly different between sequence-related and non-sequence-related units (seq. vs. non-seq. units in mixed-effect modeling of "($; &): t(34) = 1.99, p = 0.055). **c**, We calculated the interaction information (II) to examine if knowing both the count and rank about a unit's spiking within a sequence provides more information than knowing only the count or rank, namely $I(c,r;s) - I(c;s) - I(r;s)$. If so, spike count and rank provide synergistic information about the stimulus (i.e., $II > 0$). Across all 2110 units in 18 recordings, the majority of units (>95%) show a synergistic relation between spike count and rank within burst sequences. Furthermore, this synergistic relationship is significantly greater for sequence-related units as compared with non-sequence-related units (seq. vs. non-seq. units in mixed-effect modeling: $t(34) = 3.84$, $p = 0.00051$). Collectively, these data suggest that sequence-related and non-sequence-related units may be functionally different from one another. n.s. = not statistically significant. In the *left* panel of **a-c**, each *red* and *blue* dot represent results from sequence- and non-sequence-related units, respectively. In the *right* panel of **a-c**, data are shown as the mean ± s.e.m., with individual recordings shown as dots and lines color-coded by participant. N=18 recordings. Two-tailed uncorrected p-values were calculated using a linear mixed-effects model, accounting for participant-, session-, and array-level variances.

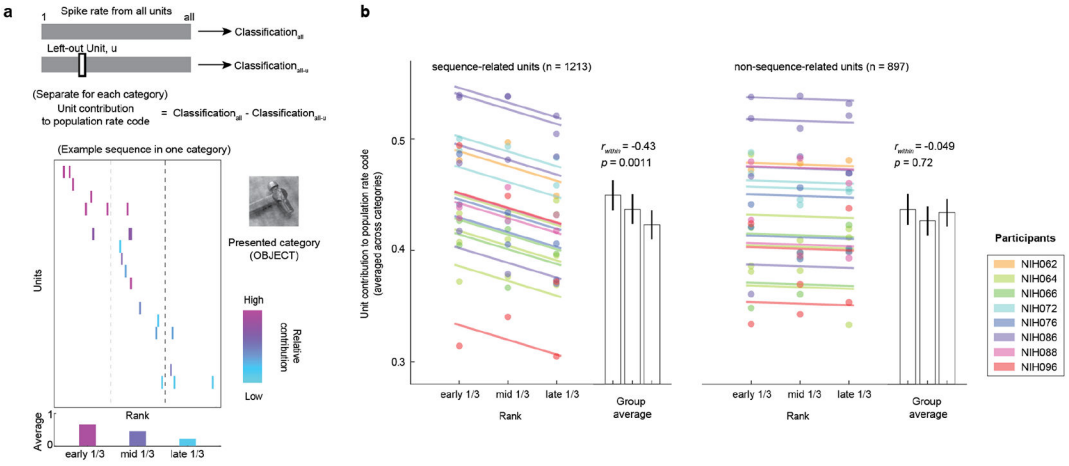

Extended Data Figure 9. Linking a unit's contribution to population rate code and its rank within neuronal sequences.

a, We assessed each unit's spike rate sensitivity to different categories by calculating the relative change in the decoding performance of a rate-based classifier when the unit is excluded. A decrease in performance upon exclusion indicates the unit's importance to the population rate code for that category. This allowed us to estimate each unit's relative contribution to population rate codes across taxonomic categories. For units within a burst, we categorized these contributions into three rank bins based on the order within category-specific template sequences. We then averaged these contributions across units and categories to explore the relationship between a unit's spiking timing and its sensitivity to visual categorical information. **b**, Across recordings and categories, units spiking earlier in a sequence contributed more to the population rate code, while later-

spiking units contributed less. This relationship was confirmed by a significant repeated-measures correlation ($r_{within} = -0.43$, $t(52) = -3.45$, $p = 0.0011$) between a unit's rank in category-specific sequences and its contribution to the population rate code, controlling for participant-, session-, or array-level variances. Non-sequence-related units, which lack reliable ranks in stimulus categories, did not show a significant relationship ($r_{within} = -0.049$, $t(52) = -0.35$, $p = 0.72$). These findings suggest that sequence-related units with firing rate responses sensitive to stimulus information tend to activate earlier within a neuronal sequence. P values are reported as two-tailed without correction.

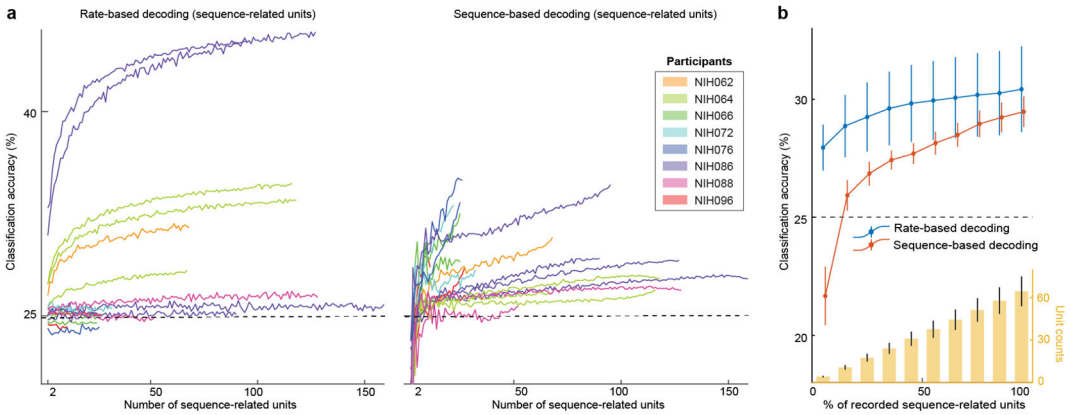

Extended Data Figure 10. Individual traces of classification accuracy for taxonomic categories as a function of included sequence-related units, separately for rate-based and sequence-based decoding.

a, The number of recorded neuronal units affects classification effect sizes. As the number of units increases, classification accuracies based on task-period spike rates and neuronal sequences during bursts both improve. Although classification accuracy based on task-period spike rates is generally higher, it appears to plateau as the number of units increases. In contrast, such a plateau is less clear for sequence-based decoding, indicating that with more recorded units, sequence-based information might continue to increase. This finding aligns with recent theories[11] and data[38] predicting that sequence-based coding could enhance coding efficiency. **b**, When data is averaged across recordings, normalizing the number of units as a percentage of total recorded units reveals similar trends. Error bars represent s.e.m., and the average number of units within each percentage bin is shown on the right y-axis. Since rate- and sequence-based classifications differ slightly in their analytical procedures, direct comparisons between them can be influenced by factors such as the number of iterations and optimization of decoding parameters. In this case, the differing slopes, rather than absolute magnitudes, of these classification outcomes suggest a potential variation in how these neural codes evolve as more neuronal units are included in the analysis.

Supplementary Material

Refer to Web version on PubMed Central for supplementary material.

Acknowledgments

We thank Robert Rosenthal and Kwabena Boahen for providing insightful comments, Michael Trotta and Anthony Jang for task development, and Alex Vaz for code and suggestions. This work was made possible by the Intramural Research Programs of the National Institute of Neurological Disorders and Stroke (ZIA-NS003144, PI: KAZ) and the NIH Pathway to Independence Award (R00NS126492, PI: WX). We are indebted to all patients who have selflessly volunteered their time to participate in this study.

Data Availability

Data used in this study are available at: https://research.ninds.nih.gov/zaghloul-lab/downloads

Code Availability

Except where otherwise noted, computational analyses were performed using custom written Matlab scripts (MathWorks, Naticks, MA). Custom code used for analysis are available at: https://research.ninds.nih.gov/zaghloul-lab/downloads.

References

1. Perkel DH & Bullock TH Neural coding. Neurosci. Res. Program Bull 6, 221–348 (1968).
2. Rieke F, Warland D, de Ruyter van Steveninck R & Bialek W Spikes: Exploring the Neural Code. (MIT Press, Cambridge, MA, 1997).
3. Shadlen MN & Newsome WT The Variable Discharge of Cortical Neurons: Implications for Connectivity, Computation, and Information Coding. 18, 3870–3896 (1998).
4. Raiguel SE, Xiao DK, Marcar VL & Orban GA Response latency of macaque area MT/V5 neurons and its relationship to stimulus parameters. J. Neurophysiol 82, 1944–1956 (1999). [PubMed: 10515984]
5. Celebrini S, Thorpe S, Trotter Y & Imbert M Dynamics of orientation coding in area VI of the awake primate. Vis. Neurosci 10, 811–825 (1993). [PubMed: 8217934]
6. Luczak A, McNaughton BL & Harris KD Packet-based communication in the cortex. Nat. Rev. Neurosci 16, 745–755 (2015). [PubMed: 26507295]
7. Nguyen ND et al. Cortical reactivations predict future sensory responses. Nature 625, 110–118 (2024). [PubMed: 38093002]
8. Tanabe S, Lee H, Wang S & Hudetz AG Spontaneous and Visual Stimulation Evoked Firing Sequences Are Distinct Under Desflurane Anesthesia. Neuroscience 528, 54–63 (2023). [PubMed: 37473851]
9. Thorpe S & Gautrais J Rank order coding. in Computational Neuroscience: Trends in Research (ed. Bower JM) 113–118 (Springer US, Boston, MA, 1998).
10. Van Rullen R & Thorpe SJ Rate coding versus temporal order coding: What the retinal ganglion cells tell the visual cortex. Neural Comput. 13, 1255–1283 (2001). [PubMed: 11387046]
11. Boahen K. Dendrocentric learning for synthetic intelligence. Nature 612, 43–50 (2022). [PubMed: 36450907]
12. Gautrais J & Thorpe S Rate coding versus temporal order coding: A theoretical approach. BioSystems 48, 57–65 (1998). [PubMed: 9886632]
13. Hahn G, Ponce-Alvarez A, Deco G, Aertsen A & Kumar A Portraits of communication in neuronal networks. Nat. Rev. Neurosci 20, 117–127 (2019). [PubMed: 30552403]
14. Palmigiano A, Geisel T, Wolf F & Battaglia D Flexible information routing by transient synchrony. Nat. Neurosci 20, 1014–1022 (2017). [PubMed: 28530664]
15. Abeles M. Corticonics: Neural Circuits of the Cerebral Cortex. (Cambridge University Press, Cambridge, UK, 1991). doi:10.1017/CBO9780511574566.

16. Bermudez-Contreras EJ et al. Formation and reverberation of sequential neural activity patterns evoked by sensory stimulation are enhanced during cortical desynchronization. Neuron 79, 555–566 (2013). [PubMed: 23932001]
17. Montijn JS, Olcese U & Pennartz CMA Visual stimulus detection correlates with the consistency of temporal sequences within stereotyped events of V1 neuronal population activity. J. Neurosci 36, 8624–8640 (2016). [PubMed: 27535910]
18. Skaggs WE, McNaughton BL, Wilson MA & Barnes CA Theta phase precession in hippocampal neuronal populations and the compression of temporal sequences. Hippocampus 6, 149–172 (1996). [PubMed: 8797016]
19. Shahbaba B. et al. Hippocampal ensembles represent sequential relationships among an extended sequence of nonspatial events. Nat. Commun 13, 1–17 (2022). [PubMed: 34983933]
20. Hahnloser RHR, Kozhevnikov AA & Fee MS An ultra-sparse code underlies the generation of neural sequences in a songbird. Nature 797, 796–797 (2002).
21. Yiling Y. et al. Robust encoding of natural stimuli by neuronal response sequences in monkey visual cortex. Nat. Commun 14, (2023).
22. Harnad S. To cognize is to categorize: Cognition is categorization. in Handbook of Categorization in Cognitive Science (eds. Cohen H & Lefebvre C) vol. 1908 19–43 (Elsevier, 2005).
23. Jang AI, Wittig JH, Inati SK & Zaghloul KA Human Cortical Neurons in the Anterior Temporal Lobe Reinstate Spiking Activity during Verbal Memory Retrieval. Curr. Biol 27, 1700–1705 (2017). [PubMed: 28552361]
24. Wittig JH, Jang AI, Cocjin JB, Inati SK & Zaghloul KA Attention improves memory by suppressing spiking-neuron activity in the human anterior temporal lobe. Nat. Neurosci 21, 808–810 (2018). [PubMed: 29786083]
25. Vaz AP, Wittig JH, Inati SK & Zaghloul KA Replay of cortical spiking sequences during human memory retrieval. Science 367, 1131–1134 (2020). [PubMed: 32139543]
26. Tong APS, Vaz AP, Wittig JH, Inati SK & Zaghloul KA Ripples reflect a spectrum of synchronous spiking activity in human anterior temporal lobe. eLife 10, 1–25 (2021).
27. Liu K, Sibille J & Dragoi G Preconfigured patterns are the primary driver of offline multi-neuronal sequence replay. Hippocampus 29, 275–283 (2019). [PubMed: 30260526]
28. Ji D & Wilson MA Coordinated memory replay in the visual cortex and hippocampus during sleep. Nat. Neurosci 10, 100–107 (2007). [PubMed: 17173043]
29. Xie W. et al. The medial temporal lobe supports the quality of visual short-term memory representation. Nat. Hum. Behav 7, 627–641 (2023). [PubMed: 36864132]
30. Nádasdy Z, Hirase H, Czurkó A, Csicsvari J & Buzsáki G Replay and time compression of recurring spike sequences in the hippocampus. J. Neurosci 19, 9497–9507 (1999). [PubMed: 10531452]
31. Reber TP et al. Representation of abstract semantic knowledge in populations of human single neurons in the medial temporal lobe. PLoS Biol. 17, 1–17 (2019).
32. Ohayon S, Freiwald WA & Tsao DY What Makes a Cell Face Selective? The Importance of Contrast. Neuron 74, 567–581 (2012). [PubMed: 22578507]
33. Resulaj A, Ruediger S, Olsen SR & Scanziani M First spikes in visual cortex enable perceptual discrimination. eLife 7, 1–22 (2018).
34. McGill WJ Multivariate information transmission. Psychometrika 19, 97–116 (1954).
35. Timme N, Alford W, Flecker B & Beggs JM Synergy, redundancy, and multivariate information measures: An experimentalist's perspective. J. Comput. Neurosci 36, 119–140 (2014). [PubMed: 23820856]
36. Kubkowski M & Mielniczuk J Asymptotic Distributions of Empirical Interaction Information. Methodol. Comput. Appl. Probab 23, 291–315 (2021).
37. Luczak A, McNaughton BL & Kubo Y Neurons learn by predicting future activity. Nat. Mach. Intell 4, 62–72 (2022). [PubMed: 35814496]
38. Sotomayor-Gómez B, Battaglia FP & Vinck M Differential population coding of natural movies through spike counts and temporal sequences. bioRxiv 1–20 (2023).

39. Gonzalo Cogno S. et al. Minute-scale oscillatory sequences in medial entorhinal cortex. Nature 625, 338–344 (2024). [PubMed: 38123682]
40. Buzsáki G & Tingley D Space and Time: The Hippocampus as a Sequence Generator. Trends Cogn. Sci 22, 853–869 (2018). [PubMed: 30266146]
41. Norman Y. et al. Hippocampal sharp-wave ripples linked to visual episodic recollection in humans. Science 365, eaax1030 (2019). [PubMed: 31416934]
42. Vaz AP, Inati SK, Brunel N & Zaghloul KA Coupled ripple oscillations between the medial temporal lobe and neocortex retrieve human memory. Science 363, 975–978 (2019). [PubMed: 30819961]
43. Norman Y, Raccah O, Liu S, Parvizi J & Malach R Hippocampal ripples and their coordinated dialogue with the default mode network during recent and remote recollection. Neuron 109, 2767–2780.e5 (2021). [PubMed: 34297916]
44. Verzhbinsky IA et al. Co-occurring ripple oscillations facilitate neuronal interactions between cortical locations in humans. Proc. Natl. Acad. Sci 121, e2312204121 (2024). [PubMed: 38157452]
45. Luczak A, Barthó P, Marguet SL, Buzsáki G & Harris KD Sequential structure of neocortical spontaneous activity in vivo. Proc. Natl. Acad. Sci. U. S. A 104, 347–352 (2007). [PubMed: 17185420]
46. Hemberger M, Shein-Idelson M, Pammer L & Laurent G Reliable Sequential Activation of Neural Assemblies by Single Pyramidal Cells in a Three-Layered Cortex. Neuron 104, 353–369.e5 (2019). [PubMed: 31439429]
47. Branco T, Clark BA & Häusser M Dendritic Discrimination of Temporal Input Sequences in Cortical Neurons. Science 329, 1671–1675 (2010). [PubMed: 20705816]
48. Pouget A, Dayan P & Zemel R Information processing with population codes. Nat. Rev. Neurosci 1, 125–132 (2000). [PubMed: 11252775]
49. Ma WJ, Beck JM, Latham PE & Pouget A Bayesian inference with probabilistic population codes. Nat. Neurosci 9, 1432–1438 (2006). [PubMed: 17057707]
50. Beck JM et al. Probabilistic Population Codes for Bayesian Decision Making. Neuron 60, 1142–1152 (2008). [PubMed: 19109917]
51. Maimon G & Assad JA Beyond Poisson: Increased Spike-Time Regularity across Primate Parietal Cortex. Neuron 62, 426–440 (2009). [PubMed: 19447097]
52. Averbeck BB Poisson or Not Poisson: Differences in Spike Train Statistics between Parietal Cortical Areas. Neuron 62, 310–311 (2009). [PubMed: 19447087]
53. Christopher Decharms R & Merzenich MM Primary cortical representation of sounds by the coordination of action-potential timing. Nature 381, 610–613 (1996). [PubMed: 8637597]
54. Gawne TJ, Kjaer TW & Richmond BJ Latency: Another potential code for feature binding in striate cortex. J. Neurophysiol 76, 1356–1360 (1996). [PubMed: 8871243]
55. Steinmetz PN et al. Attention modulates synchronized neuronal firing in primate somatosensory cortex. Nature 404, 187–190 (2000). [PubMed: 10724171]

Method References

56. Willenbockel V. et al. Controlling low-level image properties: The SHINE toolbox. Behav. Res. Methods 42, 671–684 (2010). [PubMed: 20805589]
57. Joshua M, Elias S, Levine O & Bergman H Quantifying the isolation quality of extracellularly recorded action potentials. J. Neurosci. Methods 163, 267–282 (2007). [PubMed: 17477972]
58. Thorpe S, Delorme A & Van Rullen R Spike-based strategies for rapid processing. Neural Netw. 14, 715–725 (2001). [PubMed: 11665765]
59. Farooq U, Sibille J, Liu K & Dragoi G Strengthened Temporal Coordination within Pre-existing Sequential Cell Assemblies Supports Trajectory Replay. Neuron 103, 719–733.e7 (2019). [PubMed: 31253469]
60. Chandrashekar G & Sahin F A survey on feature selection methods. Comput. Electr. Eng 40, 16–28 (2014).

61. Cohen MX Analyzing Neural Time Series Data: Theory and Practice. (MIT Press, Cambridge, MA, 2014).

62. Prechelt L. Early Stopping - But When? in Lecture Notes in Computer Science (including subseries Lecture Notes in Artificial Intelligence and Lecture Notes in Bioinformatics) vol. 7700 LECTU 55–69 (1998).

63. Estefan DP et al. Volitional learning promotes theta phase coding in the human hippocampus. Proc. Natl. Acad. Sci. U. S. A 118, 1–12 (2021).

64. Bakdash JZ & Marusich LR Repeated measures correlation. Front. Psychol 8, 456 (2017). [PubMed: 28439244]

65. Xie W & Zhang W Effortfulness of visual working memory: Gauged by physical exertion. J. Exp. Psychol. Gen (2023) doi:10.1037/xge0001391.

66. Yu Z. et al. Beyond t test and ANOVA: applications of mixed-effects models for more rigorous statistical analysis in neuroscience research. Neuron 110, 21–35 (2022). [PubMed: 34784504]

67. Rosenthal R & Rubin DB r equivalent: A simple effect size indicator. Psychol. Methods 8, 492–496 (2003). [PubMed: 14664684]

68. Xie W, Bainbridge WA, Inati SK, Baker CI & Zaghloul KA Memorability of words in arbitrary verbal associations modulates memory retrieval in the anterior temporal lobe. Nat. Hum. Behav 4, 937–948 (2020). [PubMed: 32601459]

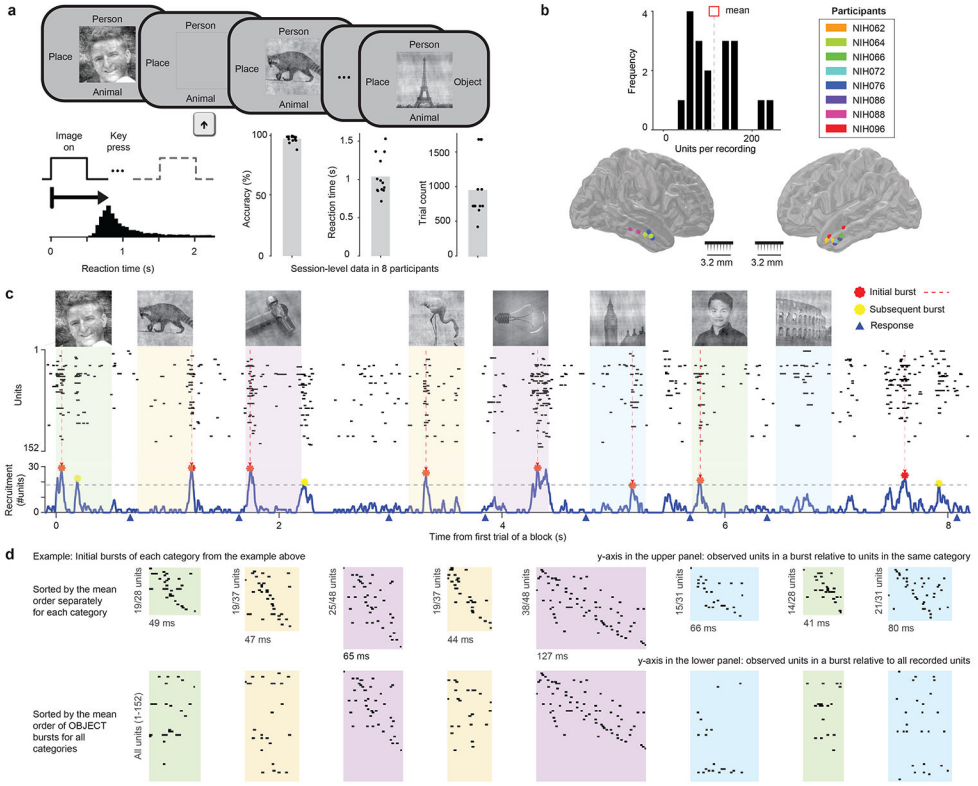

Figure 1. Spiking activity across multiple neuronal units during visual categorization in the human ATL.

a, Participants perform a visual categorization task in which they categorize the information content of a presented image into one of four options displayed on the screen. Categorization accuracy approaches ceiling within a time frame of approximately 1000 ms after stimulus onset. Each dot represents data from individual experimental sessions. **b**, During the task, we recorded single-unit spiking activity from MEAs placed in the middle temporal gyrus of the ATL. **c**, An example raster plot illustrates population spiking activity across multiple trials for a participant. Recorded units exhibit multiple bursts of activity, with several units activated close in time. Based on the number of units recruited to each burst (*lower* panel), we label the peaks of these bursts as *red* and *yellow* dots, representing the initial and subsequent bursts that occur after stimulus onset in each trial, respectively. Response timepoints are denoted by *blue* triangles. **d**, The initial burst within each trial, as depicted in **c**, is further analyzed in two ways: first, the units are sorted based on the average spiking order elicited by images from the same category (*top* panel, within-category), and then by the average spiking order of bursts associated with OBJECT images (*bottom* panel, across-category). Both sorting methods involve the same active units, but the sorting is determined by the relative order of only the overlapping units. The consistency of within-category sequences stands in stark contrast to the inconsistency observed across categories. For illustration, the photographs shown in **a** and **c** are Open Domain images or those with a copyright waiver (see Supplementary Notes). These images are similar but not identical to those used in the experiment.

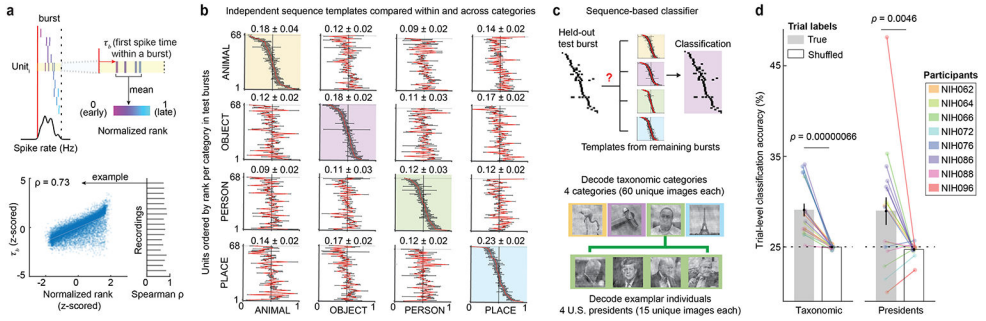

Figure 2. Decoding stimulus information from neuronal sequences in population bursts.

a, We assigned the rank of each unit within each burst based on the unit's average spike time in the burst. The normalized rank of each unit is highly correlated with the latency of the first spike from burst onset (τ_b). **b**, We identified units that exhibit a reliable rank across bursts in at least one taxonomic category (Extended Data Fig. 3a-b). Based on the retained units (e.g., 68 out of 152 in this example), we assessed the internal consistency of the order among these sequence-related units both within and across stimulus categories by sorting spiking sequences based on the units' average ranks in different folds of the data (20% per fold). In this example, the average rank-order correlation (Kendall's τ) across different data folds shown on top of each pair-wise comparison [mean ± s.e.m.] is generally higher within a category as compared with that across different categories (see Extended Data Fig. 3c for all recordings). N = 5 folds. The error bars represent s.e.m. across folds. **c**, A sequence-based classifier decodes stimulus information from a given spike sequence using category-specific templates trained on independent held-out data, separately for taxonomic and exemplar trials. **d**, In both cases, neuronal sequences carry a significant amount of information, allowing for the decoding of stimulus categories and exemplars above chance. Data are shown as the mean ± s.e.m., along with results from individual recordings shown as dots and lines color-coded by participant. N = 18 recordings. Two-tailed uncorrected p-values were calculated using a linear mixed-effects model, accounting for participant-, session-, and array-level variances. For illustration, the photographs in **c** are Open Domain images or those with a copyright waiver (see Supplementary Notes). These images are similar but not identical to those used in the experiment.

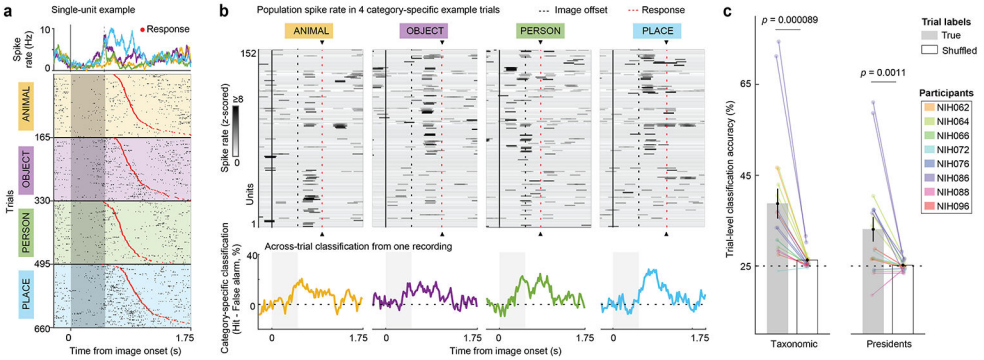

Figure 3. Decoding stimulus information from population spike rate.

a, Individual units can exhibit increases or decreases in response to the presentation of stimuli from different visual categories as demonstrated in the example. **b**, Across multiple units, changes in population spike rate can therefore be used to decode category-specific information from neural responses. The population spiking activity in one example recording captures category-specific information from the onset of the image, as revealed by the decoding outcomes of a linear logistic regression classifier (Extended Data Fig. 4a). **c**, Using the spike rate across units aggregated from a wide task-related time window (100 ms to 1400 ms), the aggregated population spike rate data can decode stimulus information across different levels of the representation hierarchy, with rate-based classification accuracies for both taxonomic and president trials significantly higher than chance. Data are shown as the mean ± s.e.m., along with results from individual recordings shown as dots and lines color-coded by participant. N = 18 recordings. Two-tailed uncorrected p-values were calculated using a linear mixed-effects model, accounting for participant-, session-, and array-level variances.

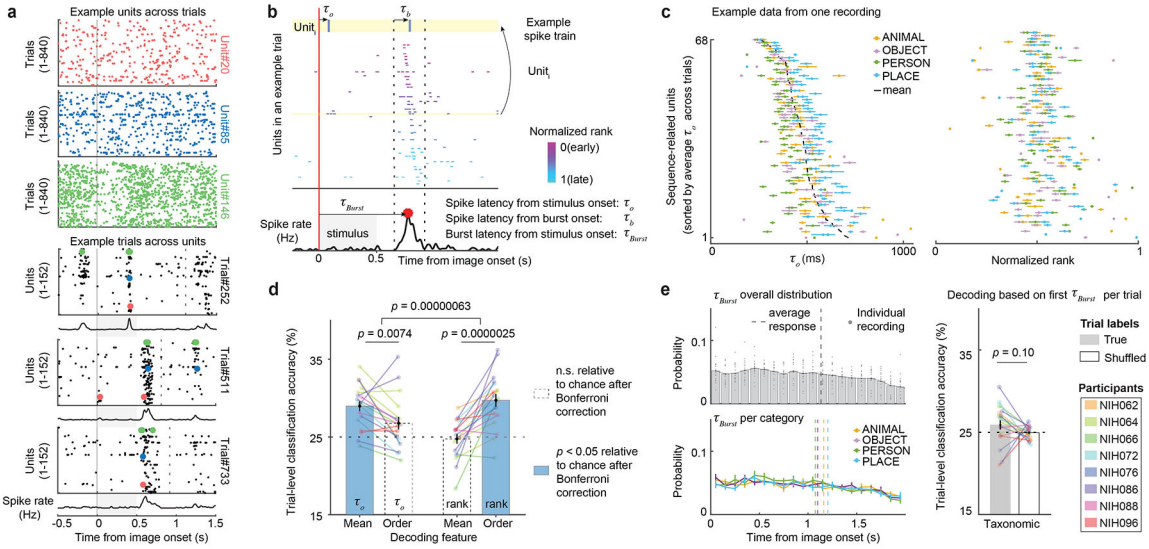

Figure 4. Spike latency and burst timing relative to stimulus onset do not capture sequence-based information within population bursts.

a, Spike raster plots from the example recording can be organized by single-unit spikes across trials (*top*) or population spikes within a trial (*bottom*). Although not every unit shows clear coordinated spike timing in conventional single-unit analysis, population activity can show temporally organized spike timing across units, manifested as bursts of population spiking. **b**, Spike timing can be assessed relative to burst onset (τ_b) and stimulus onset (τ_o). **c**, In this example, mean latency from stimulus onset, τ_o, differs between visual categories, while the relative order of τ_o across units remains consistent across caregories. In contrast, the relative rank of units within spiking bursts varies across categories, introducing variability for information coding. Data are shown as the mean ± s.e.m., along with results from individual units colored coded by category. **d**, Across trials, the average τ_o across units provides more meaningful information about visual categories than the relative order of τ_o. Conversely, the ranking of units within spiking bursts carries more stimulus information than the average rank. Solid blue bars and dashed bars indicate significant and non-significant classification accuracy relative to chance (25%) with Bonferroni correction ($p_{corrected} < .05$), respectively. **e**, Burst timing relative to stimulus onset, τ_{burst}, is evenly distributed throughout a trial (*top left*) and remains consistent across taxonomic categories (*bottom left*). The first τ_{burst} of a trial contains no decodable information for these visual categories (*right*). In **d** and **e**, data are shown as the mean ± s.e.m., along with results from individual recordings shown as dots and lines color-coded by participant. N = 18 recordings. Two-tailed uncorrected p-values were calculated using a linear mixed-effects model, accounting for participant-, session-, and array-level variances.

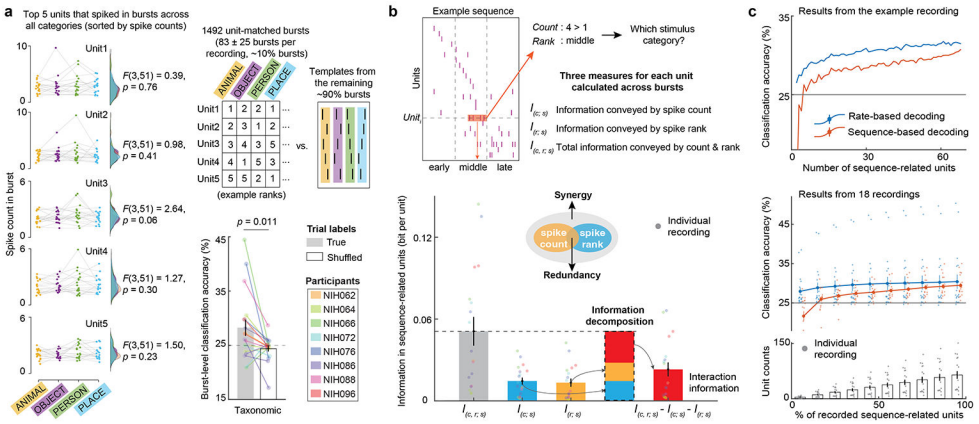

Figure 5. Spike sequence within bursts and spike rate convey distinct information about visual categories.

a, For each recording, we selected the top five sequence-related units based on the number of bursts elicited by taxonomic stimuli, ensuring that all selected units participated in these bursts. After adjusting for the overall spiking frequency of these units, we found no statistically significant difference in spike counts across categories (see Extended Data Fig. 6c for an example). Although these units exhibited similar spike rates during bursts, their ranks could still differentiate between categories, indicating a distinction between rate-based and sequence-based information. **b,** We calculated the stimulus (s) information conveyed by each unit's spike count $I(c; s)$, its relative rank $I(r; s)$, and the combination of both $I(c, r; s)$. Across recordings, sequence-related units demonstrated a significant synergistic relationship between spike count and rank, which was greater than that observed in non-sequence-related units (Extended Data Fig. 8c). **c,** In the same set of sequence-related units, both rate-based classification during the task period and sequence-based classification within bursts improved in accuracy as more units were included. Stimulus information conveyed by spike rate exceeded that of sequence-based analysis when including only a few units in a resampling analysis. However, this difference reduced as the number of included units increased. These findings were consistent in the example recording (*top*) and across all 18 recordings (*middle*), where the number of units in each recording was binned into percentiles (*bottom*, 5% to 95%; see Extended Data Fig. 10 for further discussion). Data are shown as the mean ± s.e.m., with results from individual recordings displayed as dots and lines color-coded by participant in **a** and **b** and as dots by decoding features in **c**. N = 18 recordings. Two-tailed uncorrected p-values were calculated using a linear mixed-effects model, accounting for participant, session, and array-level variances.